

**NASA TECHNICAL  
MEMORANDUM**

NASA TM X-2974



NASA TM X-2974

**CASE FILE  
COPY**

**DISTRIBUTED POROUS THROAT  
STABILITY BYPASS TO INCREASE  
THE STABLE AIRFLOW RANGE  
OF A MACH 2.5 INLET WITH  
60-PERCENT INTERNAL CONTRACTION**

*by Robert J. Shaw, Glenn A. Mitchell,  
and Bobby W. Sanders*

*Lewis Research Center  
Cleveland, Ohio 44135*



1. Report No. <b>NASA TM X-2974</b>		2. Government Accession No.		3. Recipient's Catalog No.	
4. Title and Subtitle <b>DISTRIBUTED POROUS THROAT STABILITY BYPASS TO INCREASE THE STABLE AIRFLOW RANGE OF A MACH 2.5 INLET WITH 60-PERCENT INTERNAL CONTRACTION</b>				5. Report Date May 1974	
				6. Performing Organization Code	
7. Author(s) Robert J. Shaw, Glenn A. Mitchell, and Bobby W. Sanders				8. Performing Organization Report No. E-7707	
9. Performing Organization Name and Address Lewis Research Center National Aeronautics and Space Administration Cleveland, Ohio 44135				10. Work Unit No. 501-24	
				11. Contract or Grant No.	
12. Sponsoring Agency Name and Address National Aeronautics and Space Administration Washington, D.C. 20546				13. Type of Report and Period Covered Technical Memorandum	
				14. Sponsoring Agency Code	
15. Supplementary Notes					
16. Abstract <p>The results of an experimental investigation to increase the stable airflow operating range of a supersonic, mixed-compression inlet with 60-percent internal contraction are presented. Various distributed-porous, throat stability-bypass entrance configurations were tested. In terms of diffuser-exit corrected airflow, a large inlet stable airflow range of about 25 percent was obtained with the optimum configuration if a constant pressure was maintained in the by-pass plenum. The location of the centerbody bleed region had a decided effect on the overall inlet performance. Limited unstart angle-of-attack data are presented.</p>					
17. Key Words (Suggested by Author(s)) Air intakes; Supersonic cruise inlets; Shock stability; Inlet bleed; Throat-bypass bleed; Throat stability bypass				18. Distribution Statement Unclassified - unlimited Category 01	
19. Security Classif. (of this report) Unclassified		20. Security Classif. (of this page) Unclassified		21. No. of Pages 40	
				22. Price* \$3.25	

\* For sale by the National Technical Information Service, Springfield, Virginia 22151

# DISTRIBUTED POROUS THROAT STABILITY BYPASS TO INCREASE THE STABLE AIRFLOW RANGE OF A MACH 2.5 INLET WITH 60-PERCENT INTERNAL CONTRACTION

by Robert J. Shaw, Glenn A. Mitchell, and Bobby W. Sanders

Lewis Research Center

## SUMMARY

An experimental investigation was conducted to evaluate the effectiveness of various distributed-porous, throat stability-bypass entrance configurations in providing an increased inlet stable airflow operating range. The inlet used for this study was an axisymmetric, mixed-compression type with 60 percent of the supersonic area contraction occurring internally at the design Mach number of 2.50. Data were obtained at the design Mach number for three different porous throat stability bypass entrance configurations.

The superior entrance configuration tested provided the inlet with a large stable airflow operating range from an initial high-performance operating point. Maintaining a constant pressure in the bypass plenum allowed the inlet corrected airflow to be reduced by as much as 25.5 percent without incurring unstart. The location of the centerbody bleed region with respect to the oblique shock impingement point was of prime importance in affecting overall inlet performance.

## INTRODUCTION

At flight speeds above Mach 2.0 an inlet having a mixture of internal and external compression offers high performance by supplying the engine with airflow at a high pressure level while maintaining low drag. To provide optimum internal performance for this type of inlet, the terminal shock must be kept at the inlet throat. However, mixed-compression inlets suffer from an undesirable airflow characteristic known as unstart. The closer the terminal shock to the throat, the smaller the disturbance that will cause an unstart.

This airflow disturbance causes the terminal shock to move forward of the throat where it is unstable and is violently expelled ahead of the inlet cowl. This shock expulsion or unstart causes a large rapid reduction in both mass flow and pressure recovery, and thus a large thrust loss and drag increase. Inlet buzz, compressor stall, and/or combustor blowout may also occur. Obviously, an inlet unstart is extremely undesirable, not only because of the effects on the propulsion system itself, but also on the aerodynamic qualities of the aircraft. If an inlet unstart does occur, large variations of the inlet geometry are required to reestablish initial design operating conditions.

Both external airflow transients such as atmospheric turbulence and internal airflow changes such as a reduction in engine airflow demand can cause the inlet to unstart. It is desirable for the inlet to have a large enough stable margin to absorb such transients without unstating. For an internal airflow change, the inlet should provide a margin in corrected airflow below the value for optimum performance without incurring unstart. This margin is defined as the stable airflow operating range. Conventional mixed-compression inlets can be designed to have some stable range provided by the capacity of the performance-bleed systems. Since performance-bleed exit areas are generally fixed, this stable range may not be adequate to absorb many of the airflow transients that are encountered by a typical supersonic propulsion system. An increased stable range may be provided by operating supercritically with a resultant loss in performance. Since any loss in performance is reflected directly as a loss in thrust, supercritical operation should be avoided.

To provide the necessary stable operating range without compromising steady-state performance, the inlet can be designed to replace the throat bleed with a throat stability-bypass system capable of removing large amounts of airflow when needed. This system prevents unstarts by increasing bypass airflow to compensate for reductions in the diffuser-exit airflow demand. References 1 to 4 indicate that large increases in the stability-bypass airflow may be provided without prohibitive amounts of airflow removal during normal operation; that is, the exit area is controlled to maintain a relatively constant pressure in the stability-bypass plenum. This exit-area variation might either be provided by an active control using shock position sensors or by a passive control using pressure-activated valves at the stability-bypass exit. These pressure-activated valves open in response to the pressure rise in the stability-bypass plenum caused by the forward moving terminal shock. To be most effective, the valves should be designed to maintain a nearly constant stability-bypass plenum pressure. Using a Mach 2.5, mixed-compression inlet with 40-percent internal contraction, reference 2 reported that several types of stability-bypass entrance configurations were capable of producing a large stable airflow range if a constant-pressure stability-bypass exit control could be used. When these entrance configurations were used with pressure-activated valves (see refs. 3 and 4), the diffuser-exit airflow could be reduced by as much as 28 percent from the optimum performance point without causing inlet unstart.

Experimental tests were conducted in the Lewis 10-by 10-Foot Supersonic Wind Tunnel to continue the evaluation of stability-bypass systems. The same types of stability-bypass systems as used in references 2 to 4 were investigated using an axisymmetric, Mach 2.5, mixed-compression inlet having 60 percent of the design supersonic area contraction occurring internally. Stability-bypass airflow was removed from the cowl side of the inlet throat region through several different entrance configurations. These entrance configurations used either a distributed porous surface, distributed educated slots, or a forward-slanted slot. The purpose of this report is to present the performance of the distributed porous entrance configurations and to determine its suitability for use with pressure-activated valves designed to have a nearly constant pressure characteristic.

The performance of the distributed educated and forward-slanted slot configurations are reported in references 5 and 6, respectively. Remotely variable choked-exit plug assemblies were used to vary the stability-bypass flow for the study reported herein. Data were obtained at a free-stream Mach number of 2.50 and at a Reynolds number, based on inlet cowl lip diameter, of  $3.88 \times 10^6$ . Some data were also obtained at the maximum angle of attack before unstart.

U.S. Customary Units were used in the design of the test model and for the recording and computing of experimental data. These units were converted to the International System of Units for presentation in this report.

## SYMBOLS

A	flow area, $m^2$
$A_c$	cowl lip capture area, $0.1758 m^2$
AI	airflow index, $AI = 100 \left\{ 1 - \left[ (W \sqrt{\theta/\delta})_{\min s} / (W \sqrt{\theta/\delta})_{op} \right]_5 \right\}$ , percent
$D_5$	steady-state distortion, $\left[ (P_{\max} - P_{\min}) / P_{av} \right]_5$
d	distance from local surface, cm
H	annulus or rake height, cm
M	Mach number
$m/m_0$	mass-flow ratio
P	total pressure, $N/m^2$
p	static pressure, $N/m^2$
$R_c$	inlet cowl lip radius, 23.66 cm
r	radius, cm

$SI_{cp}$	constant pressure stability index, $SI_{cp} = 100 \left\{ 1 - \left[ (W \sqrt{\theta/\delta})_{\min s, cp} / (W \sqrt{\theta/\delta})_{op} \right]_5 \right\}, \text{ percent}$
$T$	total temperature, K
$W$	airflow, kg/sec
$W \sqrt{\theta/\delta}$	corrected airflow, kg/sec
$x$	axial distance from cone tip, cm
$\alpha$	angle of attack, deg
$\delta$	$P/(10.13 \times 10^4 \text{ N/m}^2)$
$\theta$	$T/288.2 \text{ K}$
$\theta_l$	cowl lip position parameter, $\tan^{-1} \left[ 1/(x/R_c) \right]_{\text{cowl lip}}$
$\varphi$	circumferential position, deg

Subscripts:

av	average
bl	bleed
by	overboard bypass
cp	constant pressure
fc	forward cowl
$l$	local
max	maximum
min	minimum
min s	minimum stable inlet operating point
op	operation
sb	stability bypass
x	value at distance $x$
0	free stream
5	diffuser-exit station

## APPARATUS AND PROCEDURE

### Inlet Model

The inlet used in this investigation was a Mach 2.5, axisymmetric mixed-compression type with 60 percent of the design supersonic area contraction occurring internally. The inlet capture area of 0.1758 square meter sized the inlet to match the air-flow requirements of the J85-GE-13 engine at Mach 2.5 and at a free-stream total temperature of 390 K. The inlet was attached to a 0.635-meter-diameter cylindrical nacelle, in which either the engine or a coldpipe choked-exit plug assembly could be installed in the test section of the Lewis 10-by 10-Foot Supersonic Wind Tunnel. For this study only the coldpipe was used. Figure 1 shows the test model installed in the wind tunnel test section.

Some of the basic inlet design details are presented in figure 2. Cowl and centerbody static-pressure distributions, inlet contours, and diffuser area variations are shown for the inlet design Mach number and centerbody position. External compression was accomplished with a  $12.5^\circ$  half-angle cone (fig. 3). Translation of this conical centerbody provided a varying contraction ratio to affect inlet restart. At design conditions, the cone tip oblique shock passed just ahead of the cowl lip spilling 0.25 percent of the capture mass flow. Internal compression was accomplished with the oblique shock generated by the  $0^\circ$  cowl lip and the two reflected oblique shocks plus local isentropic compression between the reflected shocks. As was pointed out in reference 8, the actual oblique shock reflection points were forward of the theoretically predicted points. The geometric throat of the inlet was located at  $x/R_c = 3.475$  inlet radii (centerbody surface) where the theoretical average supersonic Mach number was 1.239 with a total-pressure recovery of 0.988. Behind the terminal shock the theoretical recovery was 0.975 at a Mach number of 0.8125.

The subsonic diffuser consisted of an initial throat region 4 hydraulic radii long, with a  $1^\circ$  equivalent conical expansion followed by the main diffuser having an equivalent conical expansion of  $8^\circ$ . Two remotely controlled bypass systems were installed in the aft portion of the diffuser: (1) a high-response sliding-louver overboard system for shock position control and (2) a low-speed ejector bypass for engine and nozzle cooling airflow. For the data reported herein both of these bypass systems were closed. The overboard bypass system leaked about 1 percent of the capture mass flow when nominally closed. The cascades placed at the entrance of the overboard bypass cavity (fig. 3) were found in reference 9 to minimize a resonance condition in the cavity. Vortex generators were installed on the centerbody at inlet station 98.17 (fig. 3). Details of the vortex generator design are shown in figure 4.

The overall diffuser length from cone tip to compressor face was 7.72 cowl lip radii. Internal surface coordinates of the inlet in terms of the cowl lip radius are presented in

table I. A more complete discussion of the inlet design characteristics is presented in reference 8.

Bleed regions were located in the throat region of the inlet on the cowl and center-body surfaces. As shown in figure 5 the forward cowl bleed airflow was dumped directly overboard. The stability-bypass airflow (used to give the inlet a large stable airflow operating range) was removed through the entrance located on the cowl side of the throat region. Figures 3 and 5 illustrate the ducting of the stability-bypass flow through the cowling to the bypass pipes. The cowl stability-bypass and the centerbody bleed flows each used two coldpipe choked-plug assemblies. The remotely actuated plugs that were used to vary these bleed and bypass flows as well as the main duct flow are shown in figure 1(b).

The photographs and sketches of the test model show a bulky external profile. The bulky cowl was necessary to facilitate the major changes made to the stability bypass and associated ducting to vary the entrance configurations, hence it is not representative of flight-type hardware.

#### Stability-Bypass Entrance and Bleed Region

The centerbody bleed region was composed of rows of normal holes (fig. 6). There were five rows of holes aft of the inlet throat and eight rows forward of the throat. The holes in the forward rows were arranged in a concentrated staggered pattern. The intent of the staggering was to prevent axial strips of unbled surface that might induce circumferential variations in the boundary layer. Variations in the centerbody bleed pattern were accomplished by closing selected rows of holes to create centerbody bleed arrangements that were compatible with the cowl side stability-bypass entrance configurations.

The basic distributed porous stability-bypass entrance that was fabricated is shown in figure 7. Also shown in the figure is the separate forward cowl bleed region, which was mentioned previously. The design of this distributed porous bypass entrance made extensive use of the bleed characteristics information contained within references 10 to 12. These bleed characteristics and the test data reported in references 1 and 8 were used to determine the location and amount of open porous area that would provide the desired amount of stability-bypass airflow.

The distributed porous stability-bypass entrance extended across the inlet throat region (fig. 7) beginning at an  $x/R_c$  of 3.282 inlet radii, which was aft of the experimental oblique shock reflection point and extended aft of the throat to an  $x/R_c$  of 3.579 inlet radii. The bypass entrance and the forward cowl bleed region were composed of the same concentrated hole pattern used for the centerbody bleed region discussed previously. Holes were 0.318 centimeter in diameter and were drilled normal to the local inlet surface. A nominal porosity of 40 percent was achieved by locating the holes on



0.476-centimeter centers. Nominal thickness of the metal surfaces in the bleed and stability-bypass regions was equal to the hole diameter. This design provided the stability-bypass entrance with the capability of removing 20 percent of the inlet capture mass flow.

The three inlet stability-bypass entrance configurations tested are shown in figure 8. As with the centerbody bleed patterns, the various forward cowl and stability-bypass entrance patterns were constructed by closing selected rows of holes. The reasons for choosing the various configurations are presented in the RESULTS AND DISCUSSION section.

### Instrumentation

Static-pressure distributions along the top centerline of the inlet cowl and centerbody were measured by the axially located static-pressure instrumentation presented in tables II and III. The main-duct total-pressure instrumentation (fig. 9) was used to determine the local flow profiles through the inlet and subsonic diffuser. The axial locations of these total-pressure rakes are shown in figure 3. Overall inlet total-pressure recovery and distortion were determined from the six 10-tube total-pressure rakes that were located at the diffuser exit (fig. 9(b)). Each rake consisted of six equal-area-weighted tubes with additional tubes added at each side of the extreme tubes in radial positions corresponding to an 18-tube area-weighted rake.

The main duct airflow, the stability-bypass airflow, and the centerbody bleed airflow were determined from static-pressure measurements and the appropriate coldpipe choked-plug areas. Bleed flow through the forward cowl bleed region was determined from the measured total and static pressures (fig. 9(c)) and the bleed exit area.

Stability-bypass total pressure was obtained from two total-pressure rakes that were located in the bypass plenum at an  $x/R_c$  of 4.086 inlet radii. Pressures from these rakes were averaged to obtain the stability-bypass recovery. Centerbody bleed and overboard-bypass total pressures were each measured by a single probe (see fig. 9(c)).

### PERFORMANCE ANALYSIS TECHNIQUE

This section of the report introduces stylized plots (fig. 10) that are typical of actual inlet stability data to be presented later. These plots are used to explain the data presentation and to show the method used to construct a final performance plot. Various performance conditions have been labelled in figure 10 to aid in the discussion.

The stability-bypass performance is shown in figure 10(a) where the total-pressure recovery is presented as a function of the mass-flow ratio of the stability bypass. The series of straight solid lines (A'AB, C'CD, etc.) represent the bypass performance obtainable with several different fixed bypass exit areas. Corresponding inlet performance is presented in figure 10(b) by a series of standard diffuser-exit total-pressure recovery against mass-flow ratio curves. The diffuser-exit mass-flow ratio, of course, reflects the changes in bypass mass-flow ratio and also changes in forward cowl and centerbody bleed mass-flow ratios. Each solid-line curve represents the performance obtainable with a fixed bypass exit area and corresponds to the solid straight line of identical labeling in figure 10(a). Each of these curves is generated by reducing the inlet diffuser-exit corrected airflow from a supercritical value and thus causing the inlet terminal shock to move upstream until unstart occurs. By this mode of operation, loci (dashed curves) of supercritical stability-bypass airflow (A'A C'C E'E G'G) and minimum stable bypass airflow (BDFH) are obtainable. For a given bypass exit area all the supercritical inlet operating points have approximately the same bypass mass-flow and pressure-recovery values. Only when the terminal shock is in the vicinity of the stability-bypass entrance region will shock pressurization occur, causing increases in the bypass mass flow and pressure recovery toward their respective minimum stable limit values. Thus, for example, all the inlet operating points between A' and A of figure 10(b) will have the same stability-bypass performance point, which is labeled as A'A in fig. 10(a).

To assess inlet stability, it is necessary to look at the change in the diffuser-exit corrected airflow, which is a function of both diffuser-exit mass-flow ratio and total-pressure recovery. Figure 10(c) presents inlet stability, expressed as an airflow index, for the same conditions of figures 10(a) and (b). Values of airflow index (AI) represent the percent change in corrected airflow between any inlet operating condition and the minimum recorded corrected airflow at point H. Figure 10(c) thus illustrates the amount of stable margin available if the stability-bypass exit area can be varied to guide the inlet operation from any operating condition to an unstart at point H. If a fixed exit area were used to obtain the large stability-bypass airflow available at point H (fig. 10(a)), a prohibitively large amount of bypass airflow would be removed from the diffuser flow at supercritical conditions (point G). If the fixed exit area were reduced to obtain an acceptable low level of supercritical bypass airflow (point C), the amount of bypass airflow and, consequently, the stable margin at the minimum stable condition (point D) would also be reduced. Similar bypass characteristics are reported in references 1 to 4.

Data such as that presented in figures 10(a) to (c) show the characteristic performance of an inlet with a stability-bypass entrance. Since a performance assessment from these plots is difficult, a single operating line was chosen to represent the configuration performance. One end of the line represents a high-performance operating point that matches the inlet and an assumed engine and will be called the match point (point A, for example). The match point was chosen to have a high inlet recovery and a small amount

of cowl side airflow removal for boundary-layer control. The other end of the operating line (the minimum stable point) was chosen by the selection of an ideal variable exit area, one that would provide a constant pressure in the bypass plenum as the inlet operated from the match point to the minimum stable point. This variable exit area provides the maximum attainable stability (points A to M in fig. 10(a)). Reference 4 reports a pressure-activated valve that varied the stability-bypass exit area to maintain an almost constant bypass plenum pressure. Thus, the selection of a constant pressure characteristic for a stability-bypass exit control is a valid technique for assessing inlet stability performance.

The inlet stability margin that is produced by a constant-pressure bypass-exit-area control is expressed as a stability index  $SI_{cp}$ . Figure 10(d) presents the constant pressure stability index for all of the operating points of figures 10(a) to (c). Note that the selected match point stability (A to M on figs. 10(a) to (c)) is now represented by a single point A. The values of stability index at any operating point represent the percent change in corrected airflow between that point and a minimum stable point that is reached only along a line of constant stability-bypass pressure recovery (A to M in fig. 10(a)). When the inlet operating point has a stability-bypass recovery lower than that of the absolute minimum stable point (H in fig. 10(a)), the absolute minimum stable point is used to compute the stability index. Therefore, the stability index for the lower bypass recovery conditions in figure 10(d) becomes identical to the airflow index in figure 10(c). Although the stability index is defined in terms of corrected airflow, that is,

$$SI_{cp} = 100 \left\{ 1 - \frac{\left[ \left( \frac{W \sqrt{\theta}}{\delta} \right)_{\min s, cp} \right]}{\left( \frac{W \sqrt{\theta}}{\delta} \right)_{op}} \right\} \quad (1)$$

it was easier in practice to determine values of stability index directly from curves of airflow index by means of the following equation:

$$SI_{cp} = 100 \left[ \frac{(AI_{op} - AI_{\min s, cp})}{(100 - AI_{\min s, cp})} \right] \quad (2)$$

where  $AI_{op}$  is the airflow index at any inlet operating condition and  $AI_{\min s, cp}$  is the airflow index at the corresponding minimum stable point assuming a constant bypass recovery is maintained.

Constant-pressure stability index levels may be converted into typical inlet performance plots like that of figure 10(g) by means of figures 10(e) and (f). Figure 10(e)

presents the constant pressure stability index that was computed for each inlet operating condition as a function of inlet total-pressure recovery. A selected inlet total-pressure recovery may be represented on figure 10(e) as a vertical line (IJKL). (Note that point A is no longer necessarily the selected match point. The choice of inlet recovery and the amount of performance bleed will dictate the match point.) The intersection of this line with the lines of constant bypass exit area indicate the constant-pressure stability indices available at the selected inlet recovery for the various bypass exit areas. A replot of these data in figure 10(f) shows the amount of stability margin that is available when operating the inlet at the selected match recovery as a function of the various amounts of initial total forward cowl bleed and stability-bypass mass flow. Any of the data points in figure 10(f) may be converted into a typical inlet performance plot. Point J, for example, is shown in figure 10(g) and is determined by the previously selected inlet recovery and the initial amount of total mass flow removed through the cowl surface. If point J represents critical inlet performance, then supercritical performance is represented by a vertical line extended below point J. The constant-pressure stability index for point J as determined by equation (1) is represented by the airflow difference between two corrected airflow lines: one through the selected match point  $(W\sqrt{\theta/\delta})_{op}$  and the other  $(W\sqrt{\theta/\delta})_{min s, cp}$  intersecting the locus of minimum stable conditions on the inlet performance map (fig. 10(b)). For convenience, inlet performance between the match point and the minimum stable point is represented by a straight line. Intermediate points could be determined by using figures 10(a) to (d).

## RESULTS AND DISCUSSION

The results of this investigation are reported in two parts: the stability performance of the configurations and, the unstart angle-of-attack performance of the configurations.

### Stability Performance

The three porous configurations that were tested are shown in figure 8. Configuration NH-1 had all 18 rows of stability bypass holes open along with the two aft most rows of forward cowl bleed holes. These two rows were located just downstream of the experimental oblique shock reflection point. The centerbody bleed pattern was identical to that of configuration A of reference 8. This configuration exhibited the best inlet total-pressure recovery performance of all the configurations reported in reference 8.

Figure 11 presents the performance characteristic curves for configuration NH-1. Cowl and centerbody surface static-pressure distributions and total-pressure profiles at the various survey stations are presented for configuration NH-1 in figure 12 for the

minimum stable operating conditions and in figure 13 for representative supercritical operating conditions. Only the profiles for rake 5 of the six diffuser-exit rakes will be presented herein as this profile was representative of those of all rakes. Note that throughout this report an attempt has been made to maintain consistency in the figure symbols; that is, the same symbol used to represent a particular fixed bypass exit area in the stability bypass performance curves (e.g., fig. 11(a)) has been used in the accompanying inlet performance curves (e.g., figs. 11(b) to (i)) and in the pressure distribution and profile figures (e.g., figs. 12 and 13).

The stability-bypass performance curves of figure 11(a) reveal a precipitous dropoff in minimum stable pressure recoveries for mass-flow ratios in excess of 0.09. This abrupt change in the stability-bypass characteristics is also manifested in the diffuser-exit performance curves of figure 11(b) where the corresponding minimum stable pressure recovery dropped by about 0.02 and in the inlet steady-state distortion curves of figure 11(i) where the distortion parameter increased by about 0.04 for the respective conditions. The resulting loss in inlet stability can be seen in figure 11(f) where rather low values in stability index were achieved at the higher mass-flow ratios.

A survey of the throat-exit rake profiles for minimum stable operation (fig. 12(d)) and supercritical operation (fig. 13(d)) indicates that a flow separation from the centerbody surface occurred in the throat region for operating conditions corresponding to the higher stability bypass flows. The separation appeared to be present regardless of terminal shock position. A comparison of the throat-exit rake profiles with the corresponding operating points on the stability-bypass performance curves (fig. 11(a)) indicates that separation occurred in conjunction with the loss in bypass pressure recovery, that is, for bypass mass flows in excess of about 0.09. The corresponding diffuser exit rake profiles (figs. 12(f) and 13(f)) reveal the flow had reattached before reaching the engine face.

Apparently this separation was caused by the large amount of flow removed through the cowl surface. The particular centerbody bleed pattern was not able to maintain attached flow at the higher stability bypass flows. The corresponding cowl static-pressure distributions of figure 12(a) indicate that the separation prohibited the terminal shock from being positioned as far forward before unstart as it could at the lower bypass flows. The more downstream positioning of the shock resulted in the lower bypass pressure recoveries achieved.

At the lower stability-bypass flows a local centerbody boundary-layer flow separation was indicated by the boundary-layer rake profiles (fig. 12(c)) for inlet operation at minimum stable conditions. This separation appeared to be identical to the phenomenon reported in reference 8 and was of such a small scale nature that it did not degrade inlet performance.

The rather poor stability performance exhibited by configuration NH-1 at the higher stability-bypass flows makes it an unacceptable configuration. Obviously if the large -

scale separation at the increased stability-bypass flows could be eliminated, a large increase in stability performance would be realized. In an attempt to eliminate the large-scale separation, the centerbody bleed pattern was altered to that corresponding to configuration NH-2. As shown in figure 8 all the centerbody bleed holes aft of the experimental shock impingement point were opened, and the forward cowl and stability-bypass hole patterns were left unchanged from those of configuration NH-1.

Figure 14 presents the performance curves for the few selected data points that were recorded for configuration NH-2. The three points shown represent the best minimum stable performance that was attained. These data points corresponded to the maximum centerbody bleed mass-flow ratio (0.07) or minimum centerbody bleed backpressure. Slightly inferior results were obtained when the centerbody bleed mass-flow ratio was a minimum (0.02).

A comparison of figure 14(a) with figure 11(a) indicates the stability bypass recoveries at minimum stable conditions were much lower for configuration NH-2 than those for NH-1 making this configuration also unacceptable from a stability performance standpoint. In the bypass mass-flow ratio range up to 0.09 the minimum stable bypass recoveries ranged from 0.48 to 0.35 for configuration NH-2 while the corresponding recovery range for configuration NH-1 was 0.60 to 0.57.

A comparison of the throat-exit rake profiles for the two configurations at minimum stable conditions (figs. 12(d) and 15(d)) indicate that the centerbody bleed configuration of NH-2 did prevent the large scale boundary-layer separation. (The diamond symbol of figure 12(d) and the triangle symbol of 15(d) represent the same stability-bypass exit area.) However, the cowl static-pressure distributions of figure 15(a) reveal that the terminal shock could not be positioned as far forward (upstream) as it could for NH-1. This downstream shock location resulted in the lower stability-bypass recoveries shown in figure 14(a). An analysis of the centerbody bleed cavity pressures measured indicates the possibility that recirculation of the centerbody bleed flow was responsible for the forward limit of the terminal shock.

Analysis of the data obtained for configurations NH-1 and NH-2 indicated that the centerbody bleed patterns were limiting the inlet stability performance that could be achieved. Configuration NH-1 had only a small centerbody bleed region, which was concentrated immediately downstream of the experimental shock impingement point ( $3\frac{1}{2}$  rows); configuration NH-2 had a large bleed region downstream of the impingement point (10 rows). To provide increased stability performance, a further change of the location of the centerbody bleed region relative to the experimental shock impingement point was incorporated into configuration NH-3. As shown in figure 8 the centerbody bleed region was located such that three rows of bleed holes were forward and three rows were aft of the experimental impingement point. In addition, the first six rows of stability-bypass holes were sealed. It should be noted that the centerbody bleed region extended upstream of the reduced stability-bypass bleed.

Before testing configuration NH-3 another configuration, which had the first three rows of stability bypass holes sealed and an identical centerbody bleed pattern to that of configuration NH-3, was tested. The performance of that configuration was almost identical to that of NH-3, and for that reason no information was included herein. These results are in agreement with those of reference 2, which reports that the location of centerbody bleed is an important factor when developing a cowl side stability-bypass system. For a given centerbody bleed pattern, significant variations in the porous stability-bypass entrance configuration did not appreciably affect the stability performance achieved.

The inlet operating characteristics for configuration NH-3 are presented in figures 16 to 18. Figure 16 presents the overall performance curves, and figures 17 and 18 present the static-pressure distributions and rake profiles for the minimum stable and representative supercritical operating conditions, respectively.

The stability-bypass performance curves of figure 16(a) reveal the best performance of the three configurations reported herein. The maximum bypass mass-flow ratio recorded was 0.21 with a corresponding bypass recovery of 0.33. The maximum bypass recovery recorded was 0.64. The diffuser-exit performance curves of figure 16(b) reveal that the total-pressure recovery increased from 0.91 to 0.94 at minimum stable conditions as the stability-bypass flow was increased. This combination of high diffuser-exit pressure recovery levels and large amounts of stability-bypass flow enabled this configuration to maintain large values of stability index even as the amount of flow removed through the cowl surface was increased (fig. 16(f)).

The static-pressure distributions and boundary-layer rake profiles for the minimum stable conditions (figs. 17(a) to (c)) reveal similar trends as those experienced by configuration NH-1 for similar conditions. The distributions indicate that the terminal shock could be positioned well forward of the geometric throat before unstart and that the rake profiles show a disturbed boundary layer at the higher stability-bypass flows. These trends indicate the presence of a small-scale separation.

Further evidence of the more forward positioning of the terminal shock can be seen if the forward cowl bleed performance curve of figure 16(h) is examined. The bleed mass-flow ratios for configuration NH-3 at the minimum stable conditions were noticeably higher than the corresponding values for the other configurations. Increased bleed mass-flow ratio is indicative of shock pressurization.

Perhaps a further tailoring of the centerbody bleed and stability-bypass patterns could have even further improved the inlet's stability performance beyond that provided by configuration NH-3. However, no additional centerbody bleed patterns were tested, as the purpose of the study reported herein was to determine if large inlet stable operating ranges could be provided by a stability-bypass system rather than to perform a complete inlet bleed optimization study. The centerbody bleed pattern of configuration NH-3 was used for all subsequent testing as reported in references 5 to 7.

The throat-exit rake profiles for the representative supercritical operating conditions (fig. 18(d)) reveal that the centerbody boundary layer was tending toward separation for the operating condition corresponding to the diamond symbol. From the recorded data points, it appears as though the centerbody boundary layer tended toward separation for the higher stability-bypass flows for a certain range of terminal shock locations near the throat exit. No such separation trend was noted for the supercritical operating condition corresponding to the largest bypass exit area operating condition shown in figure 18(d) as the terminal shock was well downstream of the throat exit.

A comparison of the configurations using the aforementioned constant pressure stability index as presented in figure 19 further indicates the superior performance levels achieved by configuration NH-3. For comparison purposes, an initial inlet operating point corresponding to 0.89 diffuser-exit total-pressure recovery and approximately 0.02 total forward cowl bleed and stability-bypass mass-flow ratio was chosen. The 0.02 mass-flow ratio removed through the cowl provided for nominal boundary-layer control. The corresponding constant pressure stability indices for configurations NH-1 and NH-3 were 14.0 percent and 25.5 percent, respectively. Insufficient data recorded for configuration NH-2 made any comparison for this configuration impossible. Configuration NH-3 could reach a final operating point before unstart of 0.94 inlet pressure recovery and 0.76 diffuser-exit mass-flow ratio; configuration NH-1 could reach a final started operating point of only 0.92 pressure recovery and 0.85 mass-flow ratio. The corresponding stability-bypass pressure recovery levels attained were about equal, 0.45 for configuration NH-1 and 0.43 for configuration NH-3. The overall effect on stability performance of the large scale centerbody separation experienced by configuration NH-1 is evident in figure 19. The precipitous dropoff in stability-bypass recovery for NH-1 essentially limited the achievable increase in bypass mass-flow ratio to 0.09, and this limit is reflected in the higher value of diffuser-exit mass flow experienced before unstart for NH-1.

#### Unstart Angle-of-Attack Tolerance

The unstart angles of attack for various initial operating conditions for configurations NH-1 and NH-3 are indicated on the appropriate inlet performance curves (figs. 11(b) and 16(b)). No such data were recorded for configuration NH-2. The angles listed represent the maximum steady-state angle of attack the particular inlet configuration could tolerate before unstart. All angles of attack given herein corresponded to conditions of no flow through the stability bypass entrance. The only cowl side flow removal was through the forward cowl bleed region and, thus, all bleed flows were for performance purposes.



In a separate study of the same inlet but with performance bleed only as reported in reference 13, it was determined that unstarts at angle of attack were caused by an overcompression of the flow field on the leeward side of the inlet. This overcompression resulted in a local choking of the flow forward of the geometric throat and subsequent unstart. Figure 20 presents the static-pressure distributions for both the cowl and centerbody surfaces for configuration NH-3 at  $3.31^\circ$  operation for initial supercritical inlet conditions. For reference the initial  $0^\circ$  angle-of-attack operating point pressure distributions are also shown. The distributions presented are typical of all those recorded for angle-of-attack operation. The cowl surface distribution of figure 20(a) reveals a region ahead of the geometric throat where the pressure ratio rose well above the sonic value of 0.5283 (assuming isentropic conditions). In addition, the profiles indicate that the terminal shock was located well downstream of the geometric throat. Thus, it appears that a leeward side overcompression and resulting local flow choking again caused the angle-of-attack unstarts.

The unstart angles of attack that were achieved by the two configurations, NH-1 and NH-3, varied from  $3.0^\circ$  to  $3.3^\circ$ , depending on the initial inlet operating conditions. These angles are commensurate with those reported in references 8 and 13 for the same inlet with varying performance bleed configurations. Thus, it appears that the inclusion of a stability-bypass system with the required entrance region did not affect the inlet's basic angle-of-attack tolerance. This was the expected result since the overcompression and local choking occurred upstream of the stability-bypass entrance.

## SUMMARY OF RESULTS

An experimental program was conducted in the Lewis 10- by 10-Foot Supersonic Wind Tunnel to evaluate the effectiveness of various distributed porous throat stability-bypass entrance configurations in providing an increased inlet stable airflow operating range. The inlet used in this investigation was an axisymmetric, mixed-compression type with 60 percent of the supersonic area contraction occurring internally at the design Mach number of 2.50.

The following results were obtained:

1. A large stable airflow operating range could be provided for an inlet operating at a high performance condition by maintaining a nearly constant plenum pressure in an inlet stability-bypass system. From an initial inlet operating condition of 89-percent diffuser-exit pressure recovery and a total forward cowl bleed plus stability-bypass mass-flow ratio of 0.02, the diffuser-exit corrected airflow could be reduced 25.5 percent for the superior configuration prior to unstart occurring.
2. Centerbody bleed location was an important factor in the development of a cowl stability-bypass configuration which would provide a large stable airflow operating range.

3. Inlet unstart angle-of-attack tolerance for the configurations tested varied from  $3.0^{\circ}$  to  $3.3^{\circ}$ . These levels were commensurate with the results determined for the same inlet without the inclusion of any throat stability-bypass system. In all cases the unstart incurred by angle-of-attack operation resulted from local flow choking ahead of the geometric throat on the leeward side of the inlet.

Lewis Research Center,  
National Aeronautics and Space Administration,  
Cleveland, Ohio, December 12, 1973,  
501-24.

#### REFERENCES

1. Sanders, Bobby W.; and Cubbison, Robert W.: Effect of Bleed-System Backpressure and Porous Area on the Performance of an Axisymmetric, Mixed-Compression Inlet at Mach 2.50. NASA TM X-1710, 1968.
2. Sanders, Bobby W.; and Mitchell, Glenn A.: Throat-Bypass Bleed Systems for Increasing the Stable Airflow Range of a Mach 2.50 Axisymmetric Inlet with 40-Percent Internal Contraction. NASA TM X-2779, 1973.
3. Sanders, Bobby W.; and Mitchell, Glenn A.: Increasing the Stable Operating Range of a Mach 2.5 Inlet. Paper 70-686, AIAA, June 1970.
4. Mitchell, Glenn A.; and Sanders, Bobby W.: Pressure-Activated Stability-Bypass - Control Valves to Increase the Stable Airflow Range of a Mach 2.5 Inlet with 40-Percent Internal Contraction. NASA TM X-2972, 1974.
5. Shaw, Robert J.; Mitchell, Glenn A.; and Sanders, Bobby W.: Distributed Educated Throat Stability Bypass to Increase the Stable Airflow Range of a Mach 2.5 Inlet with 60-Percent Internal Contraction. NASA TM X-2975, 1974.
6. Shaw, Robert J.; Mitchell, Glenn A.; and Sanders, Bobby W.: Forward-Slanted Slot Throat Stability Bypass to Increase the Stable Airflow Range of a Mach 2.5 Inlet with 60-Percent Internal Contraction. NASA TM X-2973, 1974.
7. Mitchell, Glenn A.; Sanders, Bobby W.; and Shaw, Robert J.: Throat Stability-Bypass Systems to Increase the Stable Airflow Range of a Mach 2.5 Inlet with 60-Percent Internal Contraction. NASA TM X-2976, 1974.
8. Cubbison, Robert W.; Meleason, Edward T.; and Johnson, David F.: Effect of Porous Bleed in a High-Performance Axisymmetric, Mixed-Compression Inlet at Mach 2.50. NASA TM X-1692, 1968.

9. Coltrin, Robert E. ; and Calogeras, James E. : Supersonic Wind Tunnel Investigation of Inlet-Engine Compatibility. Paper 69-487, AIAA, June 1969.
10. McLafferty, George M. : A Stepwise Method for Designing Perforated Supersonic Diffusers. Rep. R-12133-5, United Aircraft Corp. , Nov. 17, 1949.
11. McLafferty, George M. : A Study of Perforation Configurations for Supersonic Diffusers. Rep. R-53372-7, United Aircraft Corp. , Dec. 1950.
12. McLafferty, George M. ; and Ranard, E. : Pressure Losses and Flow Coefficients of Slanted Perforations Discharging from Within a Simulated Supersonic Inlet. Rep. R-0920-1, United Aircraft Corp. , 1958.
13. Choby, David A. : Tolerance of Mach 2.50 Axisymmetric Mixed-Compression Inlets to Upstream Flow Variations. NASA TM X-2433, 1972.

TABLE I. - INLET INTERNAL SURFACE COORDINATES

(a) Centerbody

Axial distance from cone tip, $x/R_c$ , inlet radii	Radial distance, $r/R_c$ , inlet radii	Axial distance from cone tip, $x/R_c$ , inlet radii	Radial distance, $r/R_c$ , inlet radii
0	0	4.563	0.588
(a)	(a)	4.724	.566
2.885	.640	5.161	.498
2.924	.649	5.261	.481
2.952	.655	5.361	.462
3.017	.667	5.461	.444
3.081	.678	5.561	.418
3.124	.684	5.661	.409
3.178	.691	5.761	.396
3.221	.696	5.861	.373
3.237	.700	5.961	.357
3.306	.703	6.061	.341
3.349	.705	6.161	.327
3.403	.707	6.261	.313
3.435	.708	6.361	.299
3.446	↓	6.461	.285
3.457		6.561	.272
3.468		6.661	.260
3.478	.707	6.761	.250
3.489	.706	6.861	.243
3.543	.702	8.961	.240
3.596	.697	7.061	.239
3.650	.691	Cylinder	
3.865	.670	7.946	0.239
3.972	.660		
4.079	.649		
4.120	.644		
4.187	.636		
4.240	.635		
4.294	.623		
4.402	.609		

<sup>a</sup> 12.5° Half angle conical section.

TABLE I. - Concluded. INLET INTERNAL SURFACE COORDINATES

(b) Cowl


Axial distance from cone tip, $x/R_c$ , inlet radii	Radial distance, $r/R_c$ , inlet radii	Axial distance from cone tip, $x/R_c$ , inlet radii	Radial distance, $r/R_c$ , inlet radii
2.009	1.000	4.267	0.906
2.156		4.277	.905
2.297		4.384	.903
2.383		4.545	.902
2.469		4.706	.902
2.491		4.868	.903
2.512		5.029	.904
2.566		5.093	.904
2.630		5.161	.905
2.695		5.261	.907
2.738		5.361	.910
2.811	.992	5.461	.913
2.860	.989	5.561	.916
2.885	.988	5.661	.917
2.924	.986	5.761	.918
2.952	.985	Cylinder	
3.017	.981	6.235	0.918
3.081	.979		
3.124	.976	Bypass gap	
3.178	.972	6.845 6.861 6.961 7.061 7.161 7.261 7.361 7.461 7.561 7.661	0.887 .887 .885 .882 .879 .873 .868 .864 .863 .862
3.221	.971		
3.237	.966		
3.306	.963		
3.350	.960		
3.403	.955		
3.435	.953		
3.446	.952		
3.457	.951		
3.468	.951		
3.478	.950	Cylinder	
3.489	.949	7.946	0.862
3.543	.945		
3.596	.942		
3.650	.939		
3.756	.932		
3.863	.925		
3.970	.919		
4.088	.913		
4.093	.913		
4.189	.909		

TABLE II. - COWL STATIC -  
PRESSURE TAP LOCATIONS  
ALONG TOP CENTERLINE

Axial distance from cowl lip, $x/R_c$ , inlet radii		
2.983	3.439	4.254
3.090	3.474	
3.160	3.509	
3.195	3.544	
3.230	3.579	
3.264	3.620	
3.300	3.662	
3.335	3.739	
3.369	3.818	
3.404	3.969	

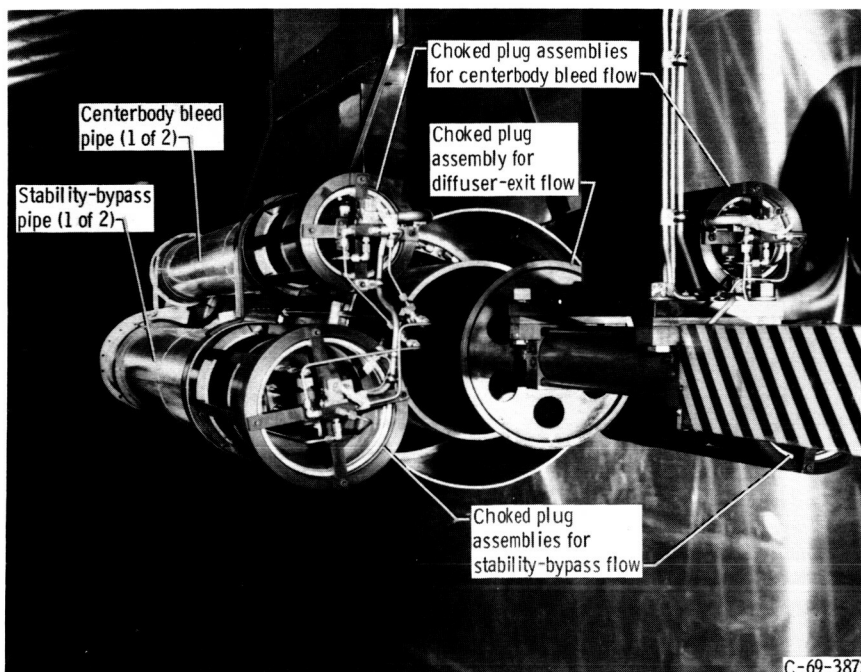
TABLE III. - CENTERBODY  
STATIC -PRESSURE TAP  
LOCATIONS

Axial distance from cowl lip, $x/R_c$ , inlet radii		
2.806	3.367	3.854
2.920	3.402	3.906
3.022	3.440	3.961
3.135	3.470	4.067
3.173	3.516	4.174
3.206	3.573	4.331
3.242	3.635	
3.272	3.691	
3.315	3.741	
3.332	3.798	



C-70-3482

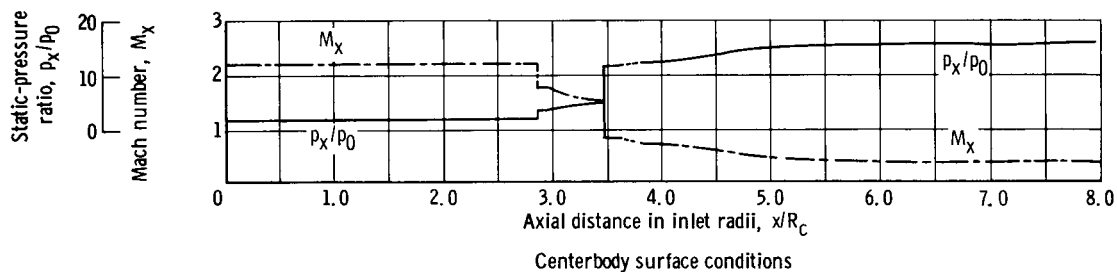
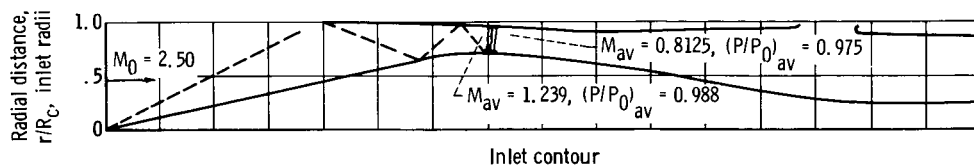
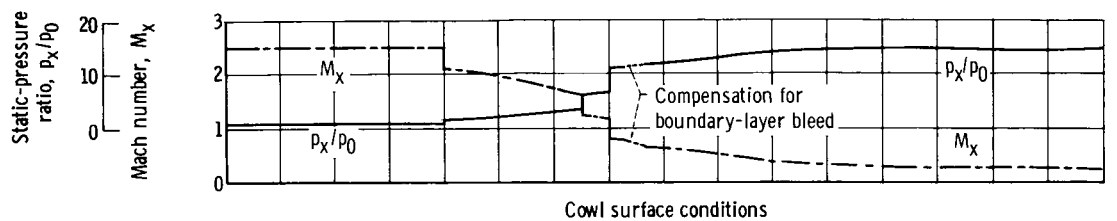
(a) Front view.



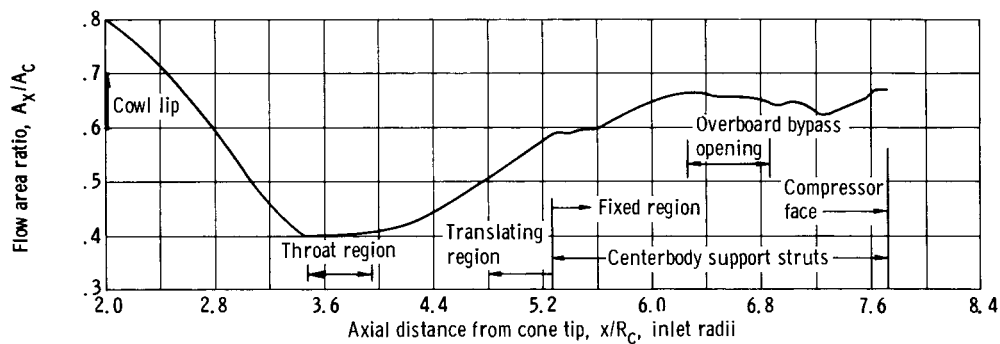
C-69-3872

(b) Rear view.

Figure 1. - Model installed in wind tunnel.



(a) Inlet dimensions and theoretical flow conditions.



(b) Diffuser area variation for  $\theta_L, 26.72^\circ$ .

Figure 2. - Aerodynamic details.



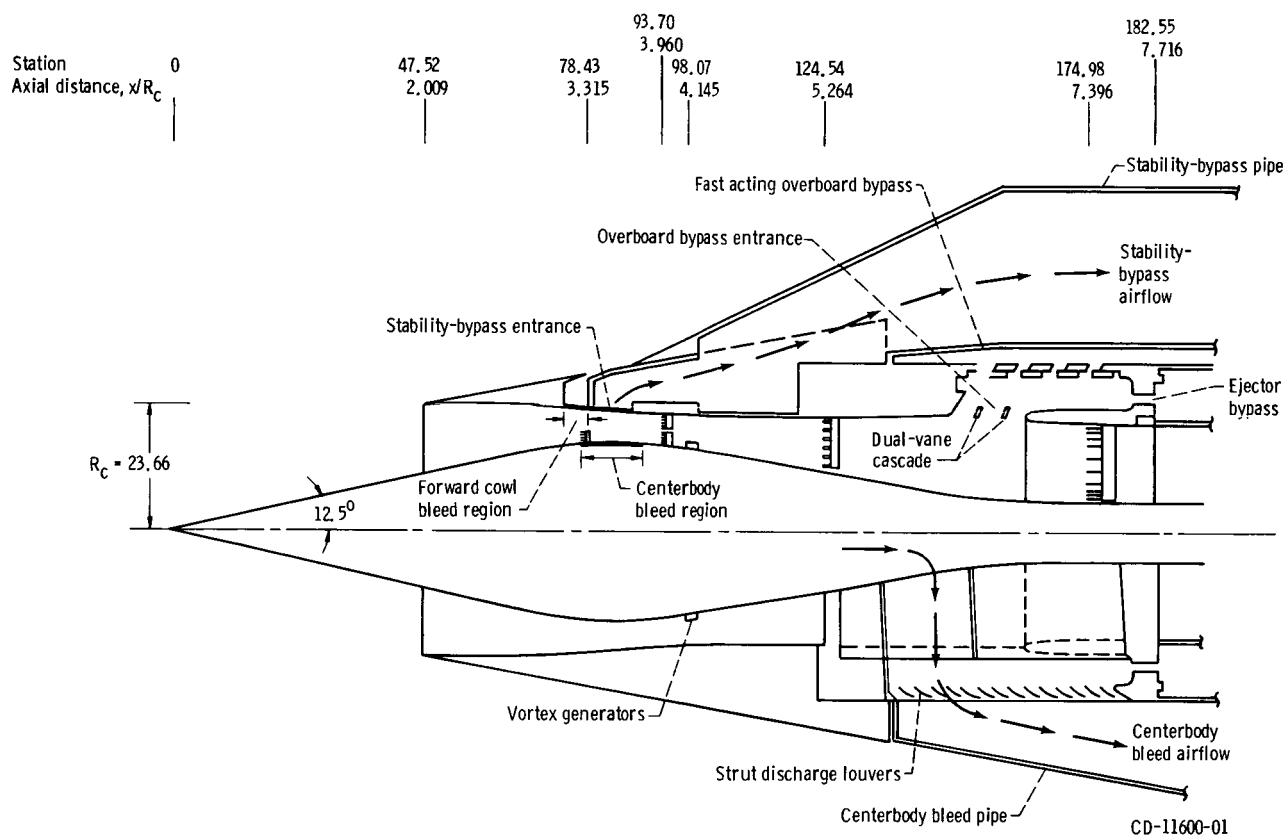


Figure 3. - Inlet details. (All linear dimensions are in cm.)

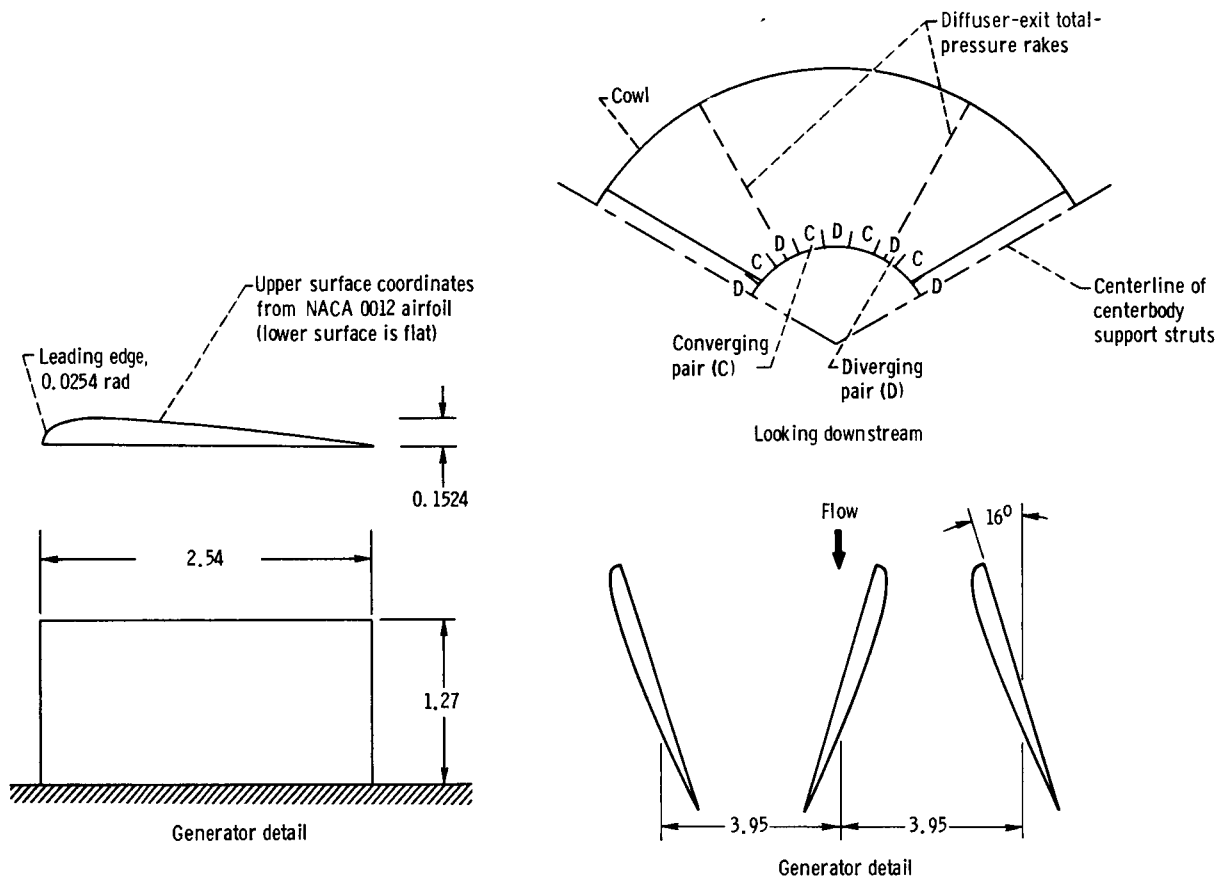


Figure 4. - Vortex generator design. (All linear dimensions are in cm.)

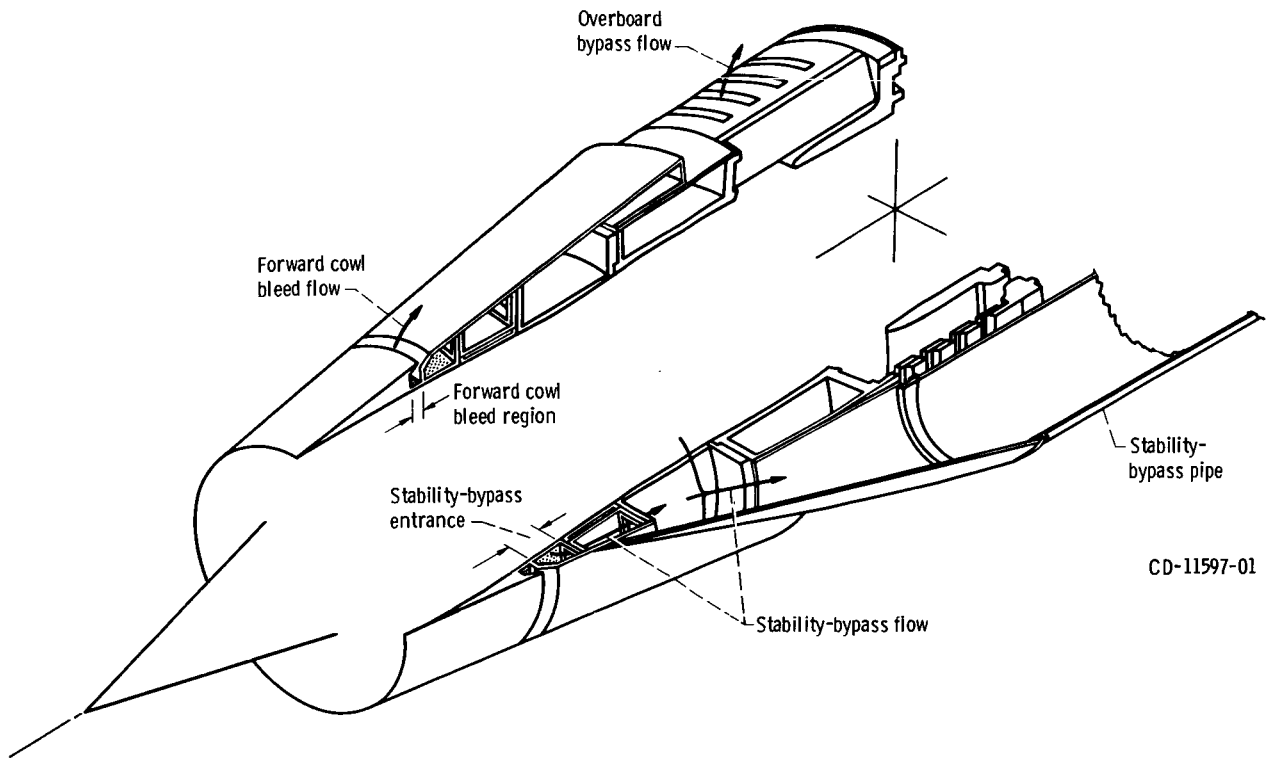


Figure 5. - Sketch of inlet cowl showing cowl bleed and bypass ducting.

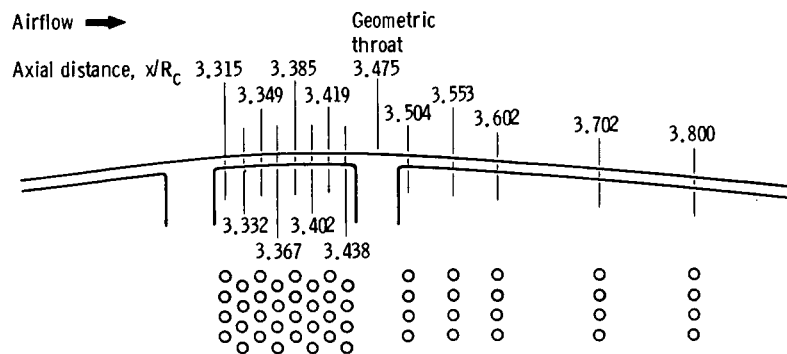


Figure 6. - Centerbody bleed arrangement. Hole diameter, 0.3175 centimeter.

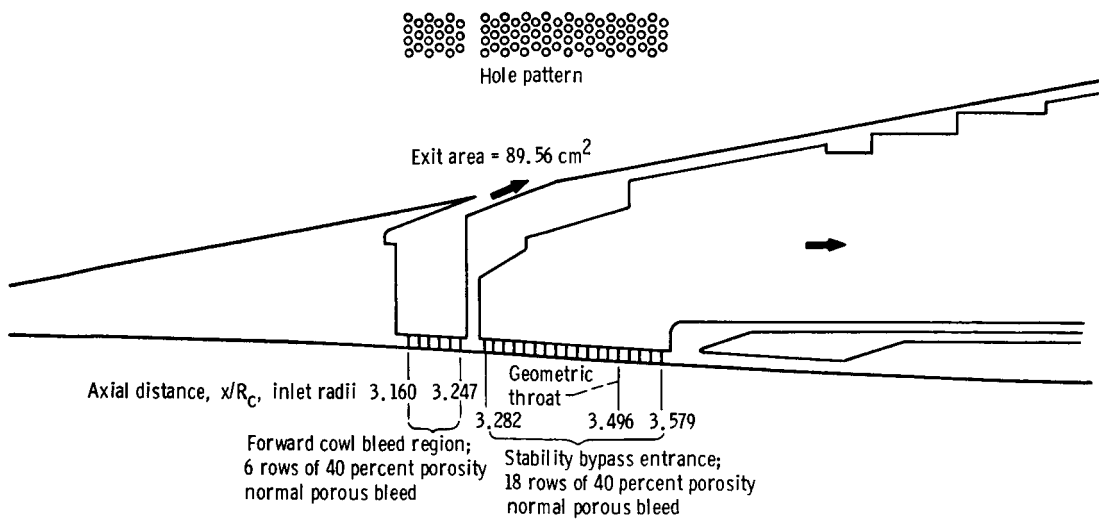
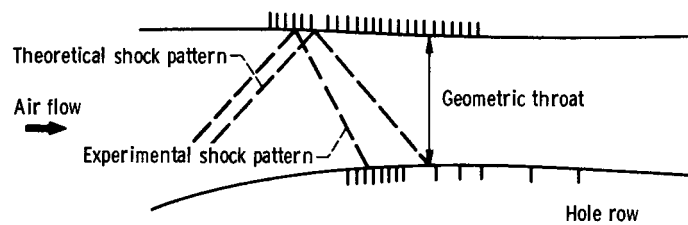


Figure 7. - Distributed porous stability-bypass entrance and forward cowl bleed region. Hole diameters, 0.3175 centimeter.

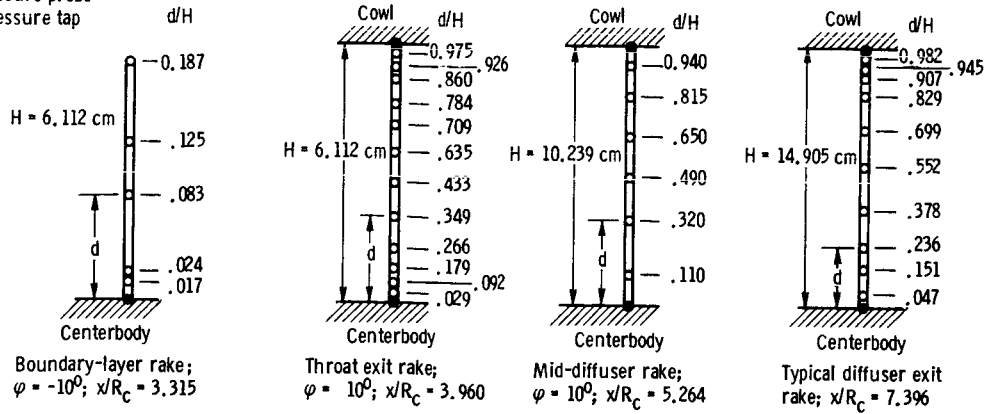


Config- uration	Forward cowl bleed region	Distributed porous stability-bypass entrance	Centerbody bleed region
NH-1	●●●●○	○○○○○○○○○○○○○○○○○○○○	●●●○○○○●●●●●
NH-2	●●●●○	○○○○○○○○○○○○○○○○○○○○	●●●○○○○○○○○○○
NH-3	●●●●○	●●●●●○○○○○○○○○○○○○○	○○○○○○○○●●●●●

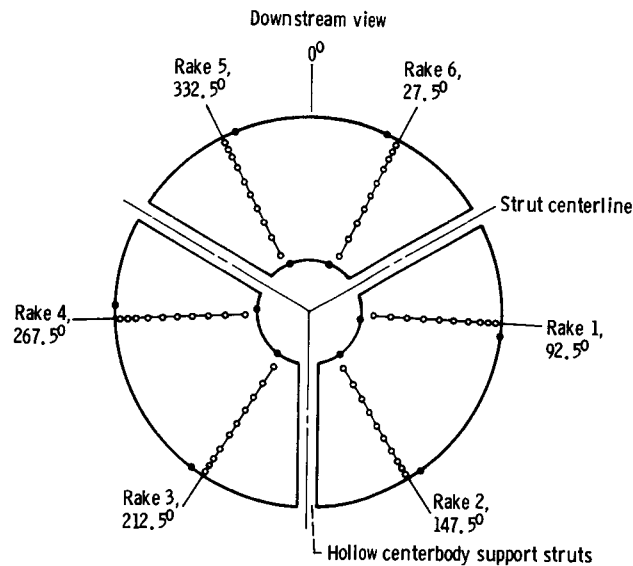
○ Row open ● Row closed ◐ Alternate holes closed

Figure 8. - Inlet stability-bypass entrance and bleed region configurations.

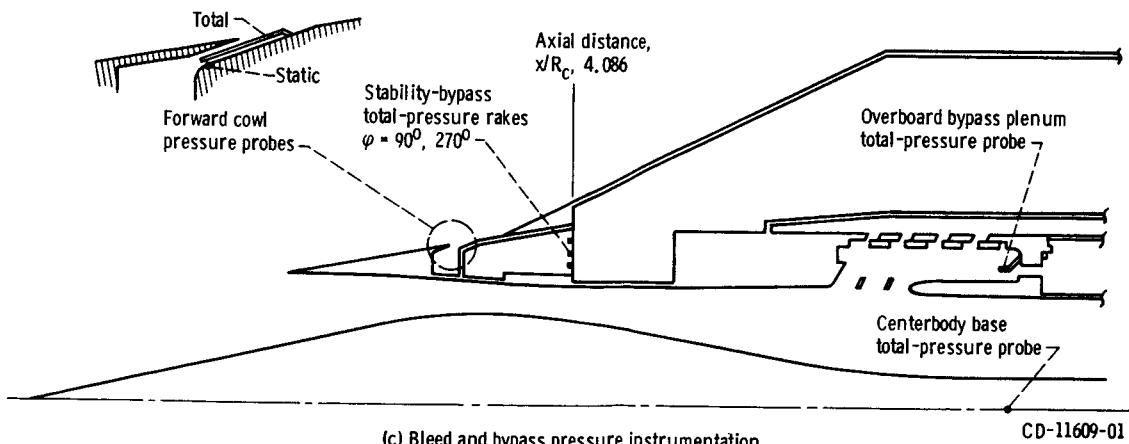
- Total-pressure probe
- Static-pressure tap



(a) Inlet-total-pressure rake dimensions.



(b) Total- and static-pressure instrumentation at diffuser-exit station,  $x/R_C = 7.396$ .



(c) Bleed and bypass pressure instrumentation.

CD-11609-01

Figure 9. - Inlet-pressure instrumentation ( $x/R_C$  is the axial distance from cone tip,  $\varphi$  is the circumferential position, and  $d/H$  is the ratio of distance from surface to annulus height).

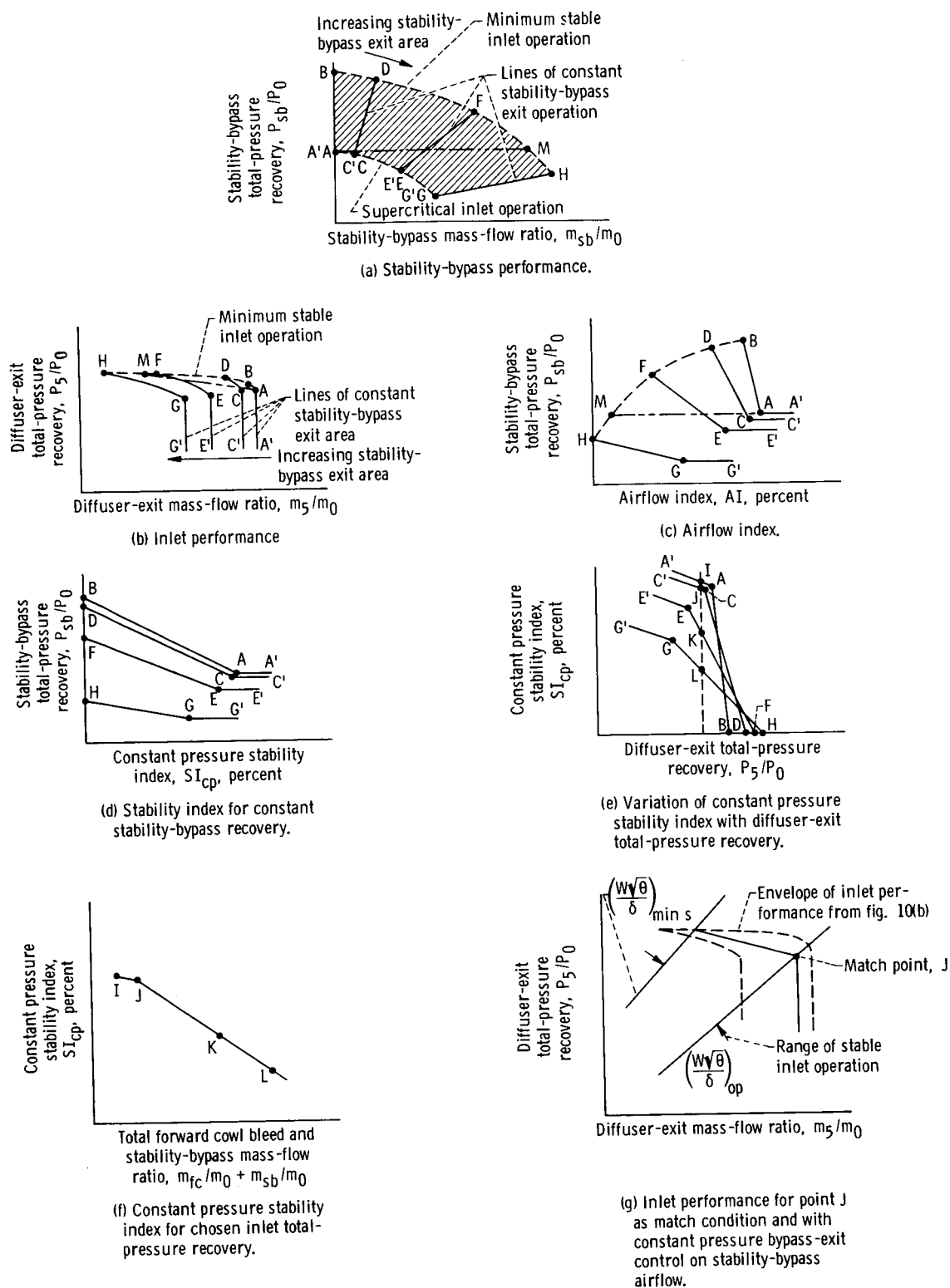


Figure 10. - Inlet stability data.

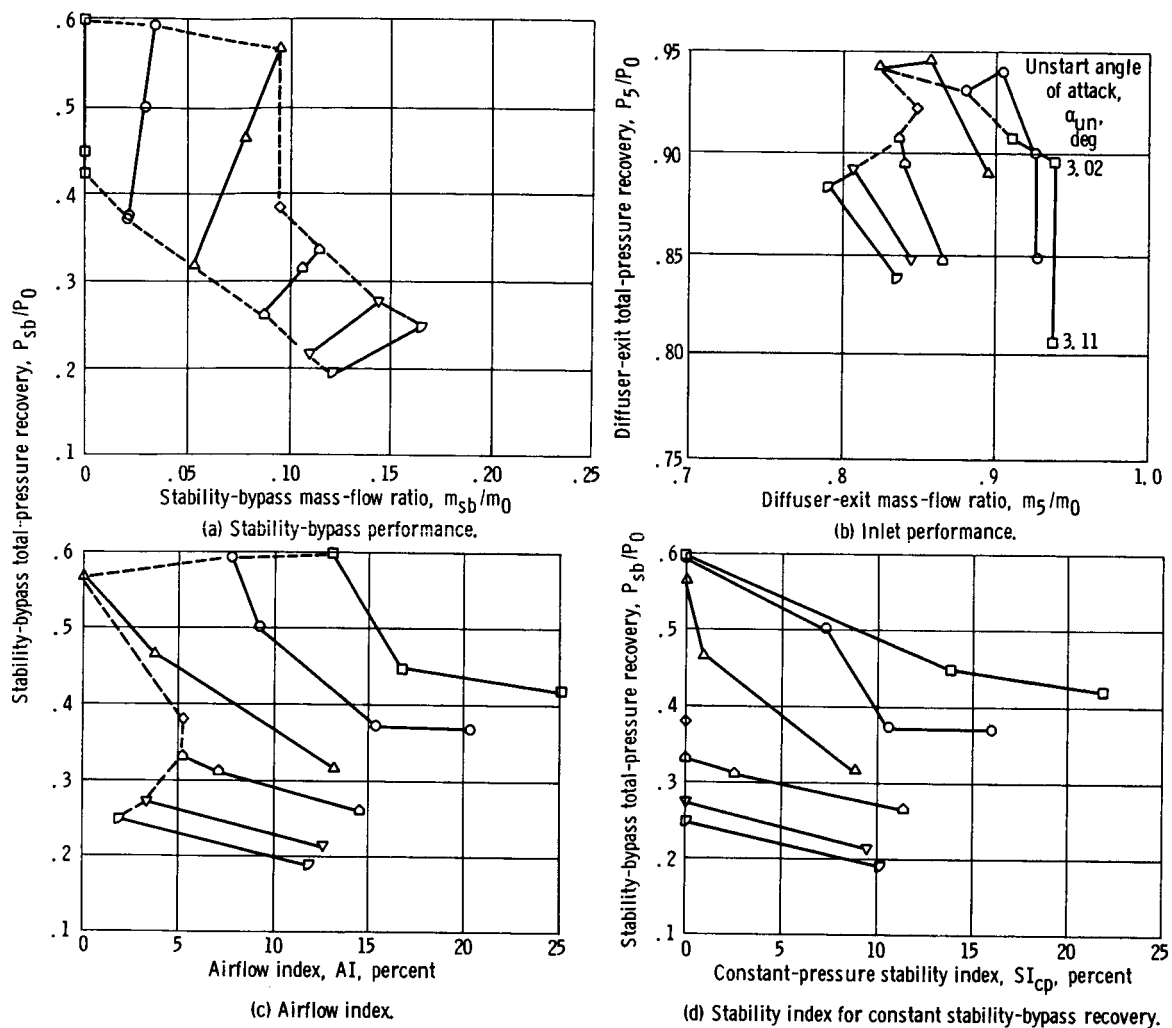
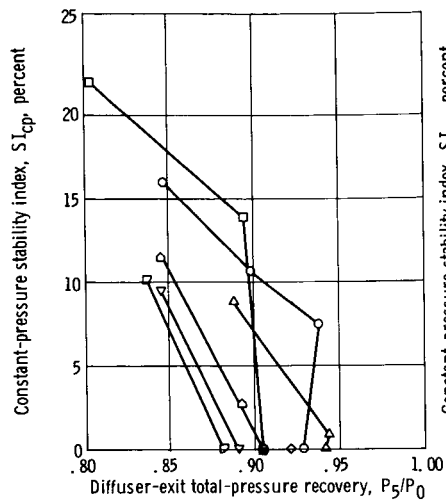
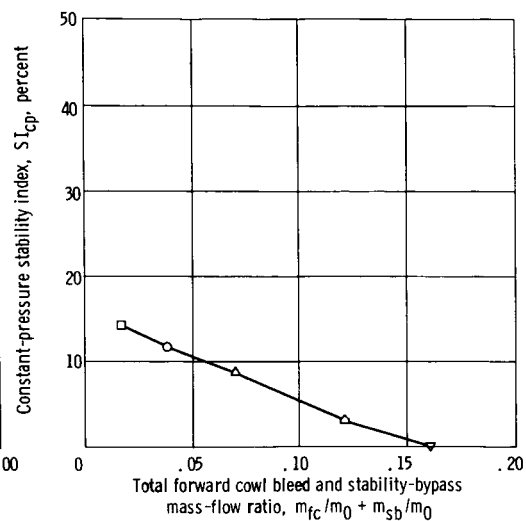


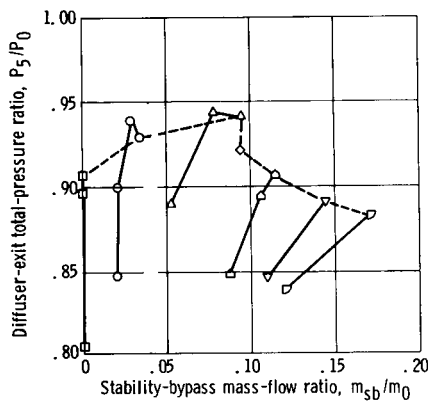
Figure 11. - Performance of distributed porous configuration NH-1. Free-stream Mach number, 2.5; angle of attack,  $0^\circ$ ; overboard-bypass mass-flow ratio, 0.01.



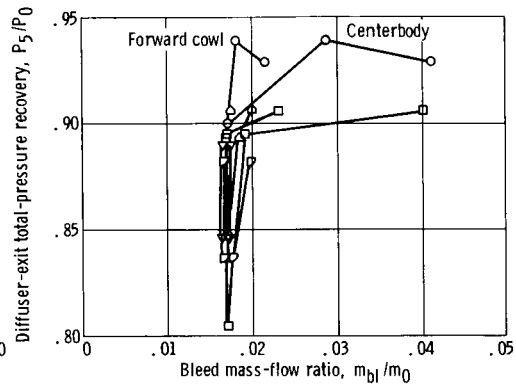
(e) Variation of constant-pressure stability index with diffuser-exit total-pressure recovery.



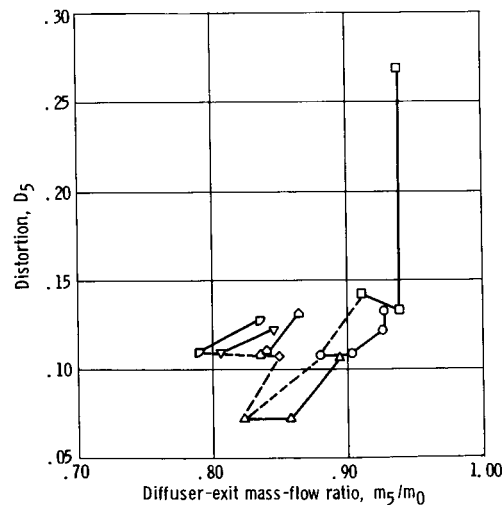
(f) Constant-pressure stability index for initial diffuser-exit total-pressure recovery of 0.89.



(g) Variation of diffuser-exit total-pressure recovery with stability-bypass mass flow.



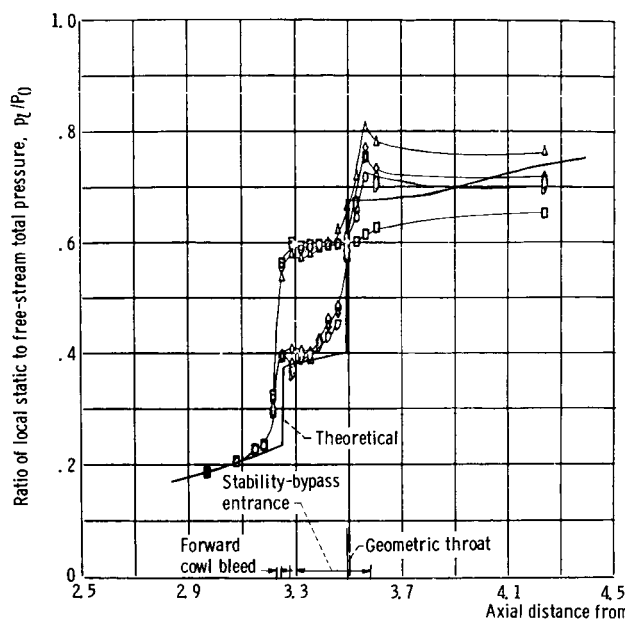
(h) Forward cowl and centerbody bleed performance.



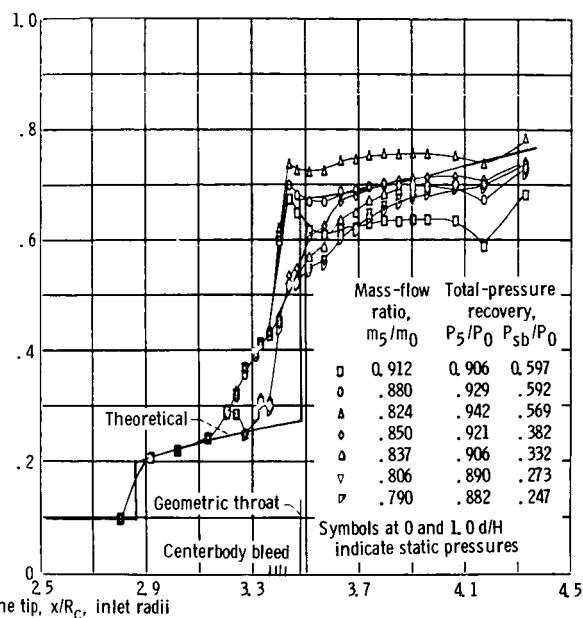
(i) Steady-state distortion.

Figure 11. - Concluded.

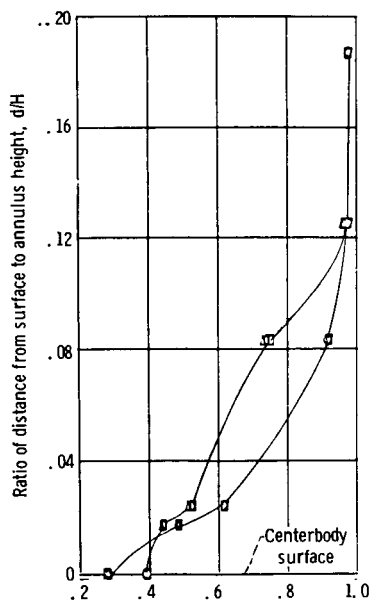




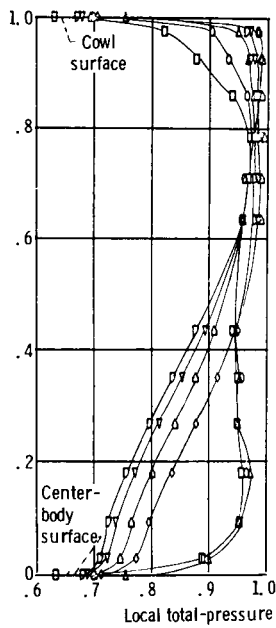
(a) Internal cowl surface pressure distributions.



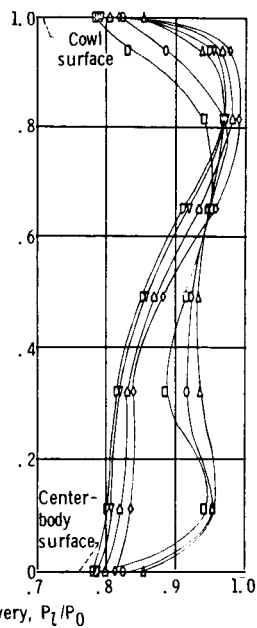
(b) Centerbody surface pressure distributions.



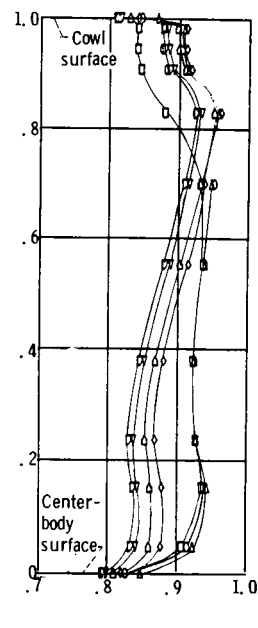
(c) Boundary-layer rake profiles.



(d) Throat-exit rake profiles.



(e) Mid-diffuser rake profiles.



(f) Typical diffuser-exit rake profiles.

Figure 12 - Diffuser static- and total-pressure distributions for configuration NH-1 at minimum stable operation.

Figure 10 is a line graph showing the internal cowl surface pressure distributions. The y-axis represents the ratio of local static to free-stream total pressure,  $P_t/P_0$ , ranging from 0 to 8. The x-axis represents the axial distance from the inlet,  $x/b$ , ranging from 2.5 to 4.5. The graph includes several data series: a solid line labeled 'Theoretical' which starts at  $x/b \approx 2.8$  and  $P_t/P_0 \approx 2.5$ , rises to a peak of  $P_t/P_0 \approx 3.5$  at  $x/b \approx 3.3$ , and then decreases; a dashed line labeled 'Geometric throat' which starts at  $x/b \approx 3.3$  and  $P_t/P_0 \approx 3.5$ , rises to a peak of  $P_t/P_0 \approx 4.5$  at  $x/b \approx 3.7$ , and then decreases; a solid line labeled 'Stability-bypass entrance' which starts at  $x/b \approx 3.3$  and  $P_t/P_0 \approx 3.5$ , rises to a peak of  $P_t/P_0 \approx 4.5$  at  $x/b \approx 3.7$ , and then decreases; and a solid line labeled 'Forward cowl bleed' which starts at  $x/b \approx 2.8$  and  $P_t/P_0 \approx 2.5$ , rises to a peak of  $P_t/P_0 \approx 3.5$  at  $x/b \approx 3.3$ , and then decreases. There are also several other data series represented by open circles, squares, and triangles, showing various pressure profiles across the axial distance.

Figure 1 is a line graph showing the centerbody surface pressure distributions. The y-axis represents the mass-flow ratio,  $m_5/m_0$ , ranging from 0 to 8. The x-axis represents the normalized axial distance,  $x/R_c$ , ranging from 2.5 to 4.5. The graph includes a 'Theoretical' curve, a 'Geometric throat' label, and 'Centerbody bleed' and 'tip,  $x/R_c$  inlet radii' labels. Symbols at 0 and 1.0 d/H indicate static pressure.

Symbol	$m_5/m_0$	$P_5/P_0$	$P_{sb}/P_0$
□	0.939	0.804	0.423
○	0.928	0.846	0.369
△	0.895	0.889	0.318
▽	0.865	0.846	0.260
◇	0.846	0.845	0.212
◇	0.836	0.837	0.191

Figure 1 is a line graph with the following data points:

Ratio of distance from surface to centerbody surface, $x/R$	Ratio of distance from surface to annulus height, $d/H$
0.0	0.20
0.2	0.20
0.4	0.20
0.6	0.20
0.8	0.20
1.0	0.20

The graph plots the recovery of surface area ( $A/A_0$ ) against the ratio of body length to head length ( $P_L/P_0$ ). The x-axis is labeled 'recovery,  $P_L/P_0$ ' and ranges from 0.6 to 1.0. The y-axis is labeled ' $A/A_0$ ' and ranges from 0 to 1.0. There are two sets of curves: one set labeled 'Cowl surface' and another set labeled 'Centerbody surface'. Each set contains multiple curves representing different fish species. The 'Cowl surface' curves generally show a peak in recovery around  $P_L/P_0 \approx 0.8$ , while the 'Centerbody surface' curves show a peak around  $P_L/P_0 \approx 0.7$ .

(c) Boundary-layer rake profiles.

(d) Throat-exit rake profiles.

(e) Mid-diffuser rake profiles.

**(f) Typical diffuser-exit rake profiles.**

**Figure 13 - Diffuser static- and total-pressure distributions for configuration NH-1 at supercritical operation.**

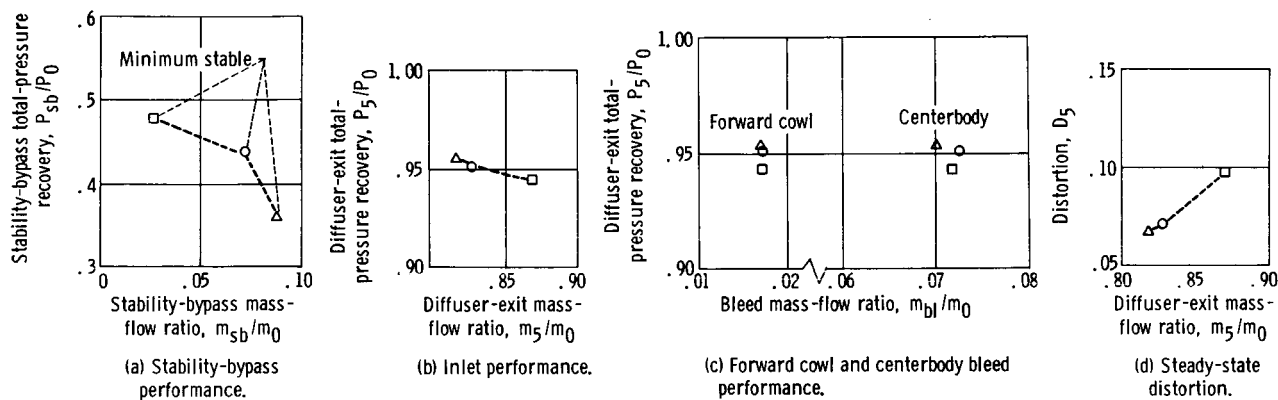
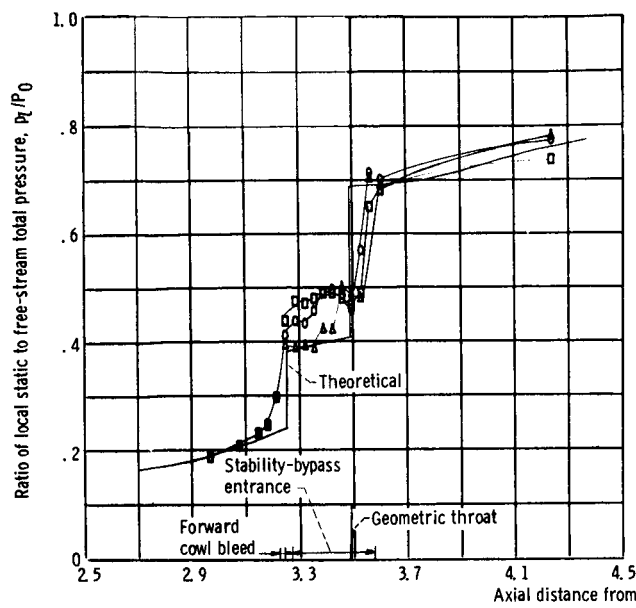
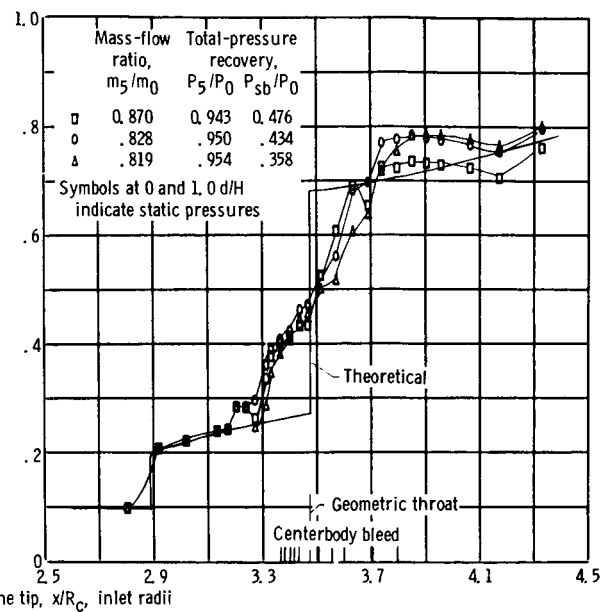


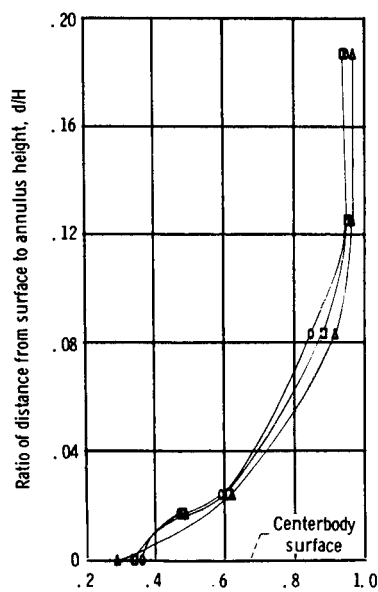
Figure 14. - Performance of distributed porous configuration NH-2. Free-stream Mach number, 2.5; angle of attack,  $0^\circ$ ; overboard-bypass mass-flow ratio, 0.01.



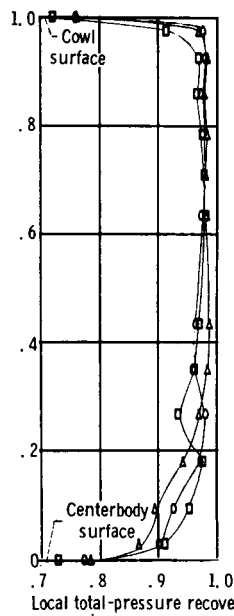
(a) Internal cowl surface pressure distributions.



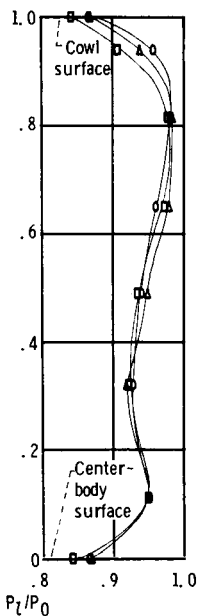
(b) Centerbody surface pressure distributions.



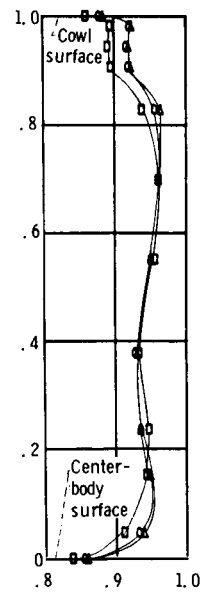
(c) Boundary-layer rake profiles.



(d) Throat-exit rake profiles.

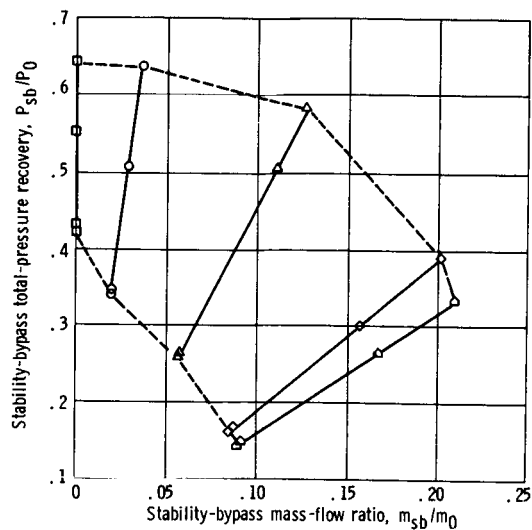


(e) Mid-diffuser rake profiles.

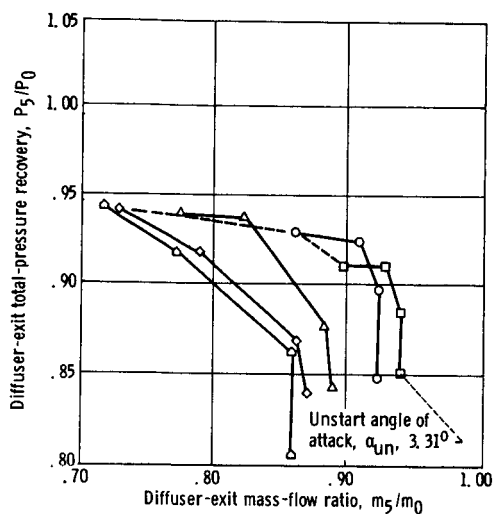


(f) Typical diffuser-exit rake profiles.

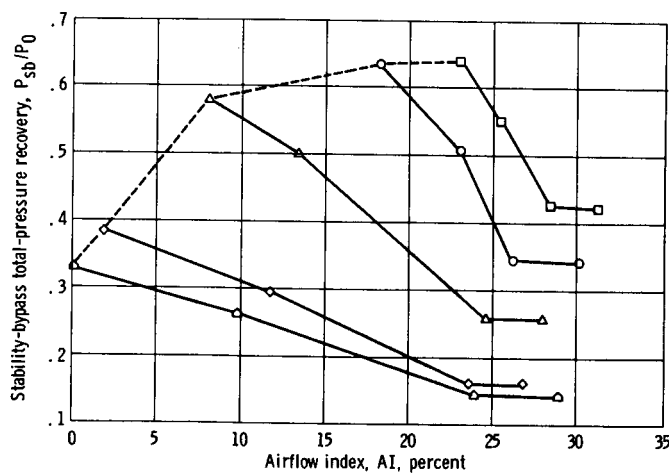
Figure 15. - Diffuser static- and total-pressure distributions for configuration NH-2 at minimum stable operation.



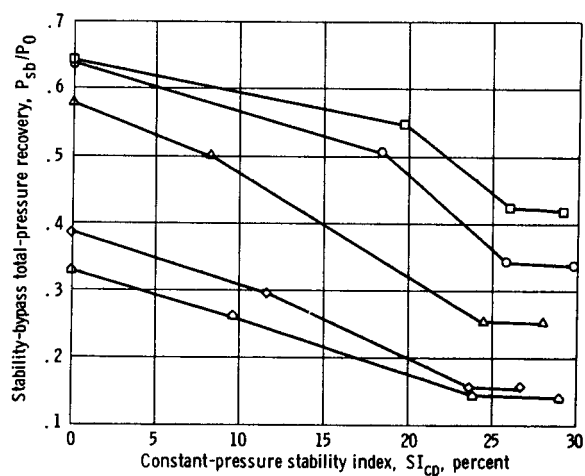
(a) Stability-bypass performance.



(b) Inlet performance.

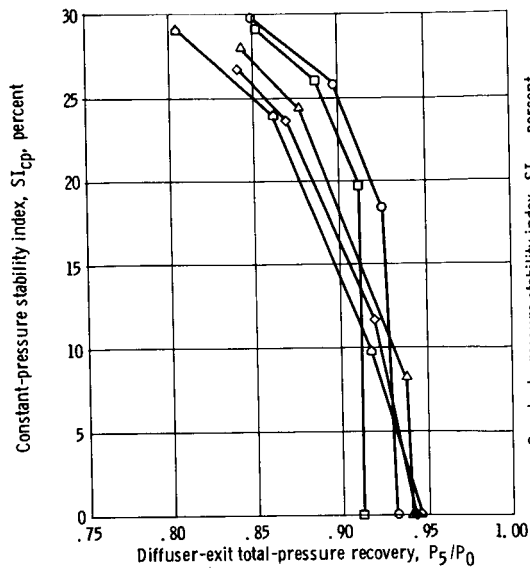


(c) Airflow index.

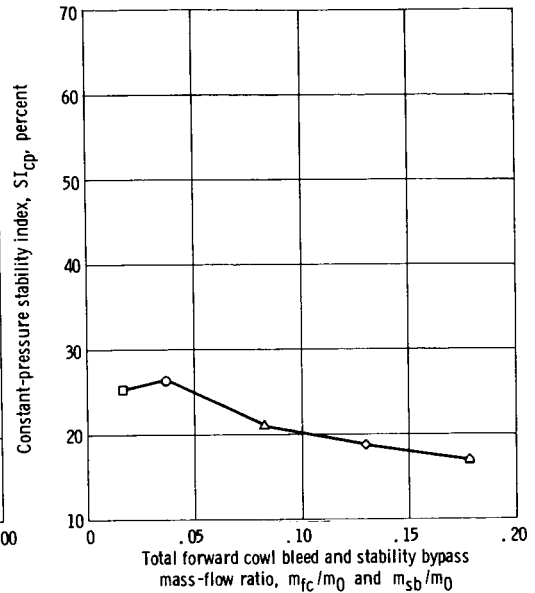


(d) Stability index for constant stability-bypass recovery.

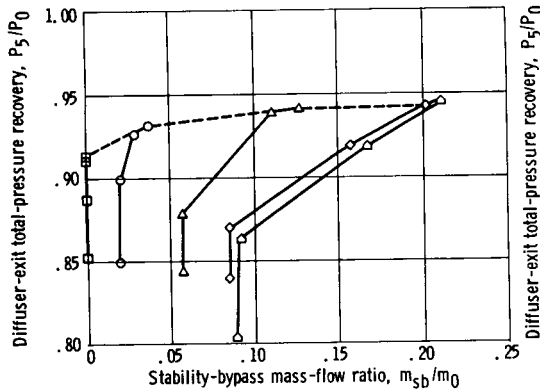
Figure 16. - Performance of distributed porous configuration NH-3. Free-stream Mach number, 2.5; angle of attack,  $0^\circ$ ; overboard-bypass mass-flow ratio, 0.01.



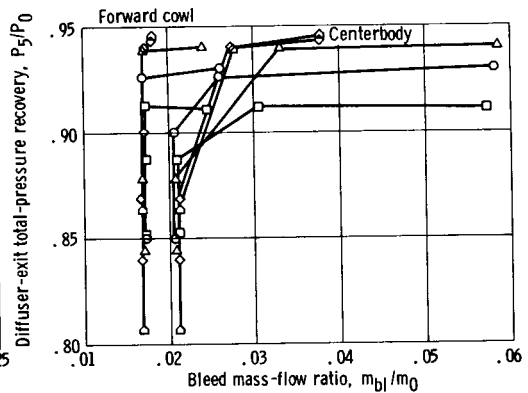
(e) Variation of constant-pressure stability index with diffuser-exit total-pressure recovery.



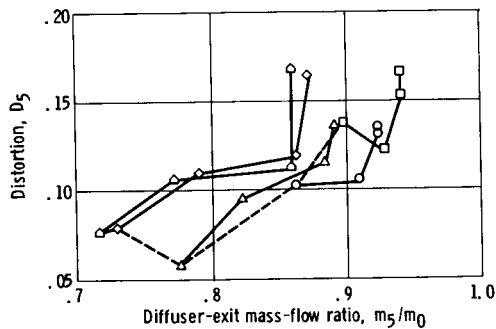
(f) Constant-pressure stability index for initial diffuser-exit total-pressure recovery of 0.89.



(g) Variation of diffuser-exit total-pressure recovery with stability-bypass mass flow.

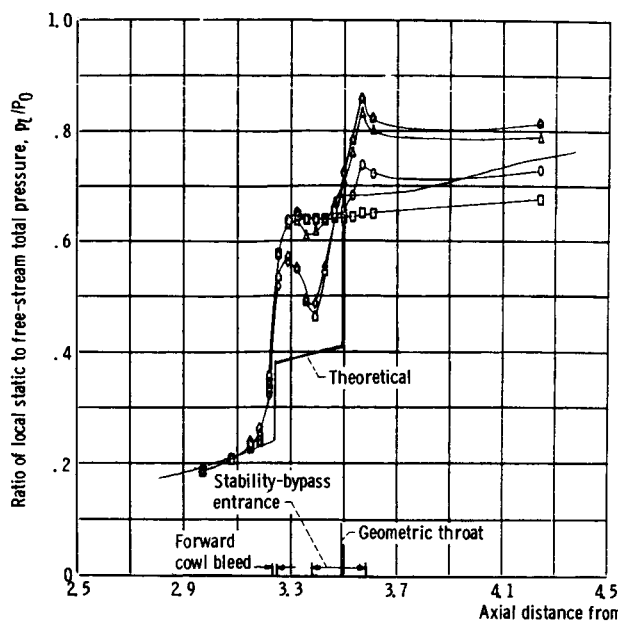


(h) Forward cowl and centerbody bleed performance.

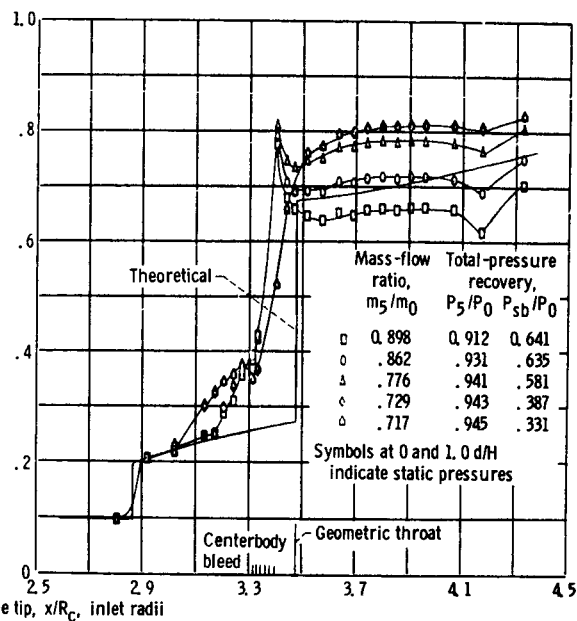


(i) Steady-state distortion.

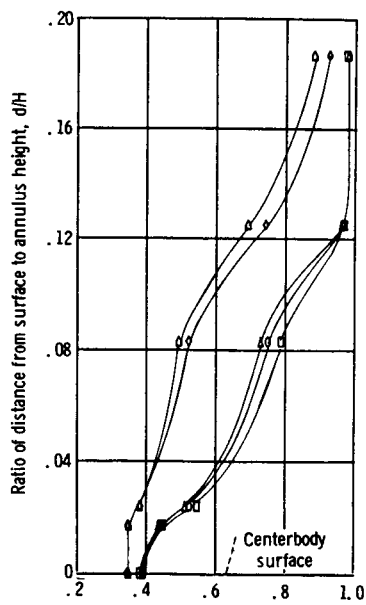
Figure 16. - Concluded.



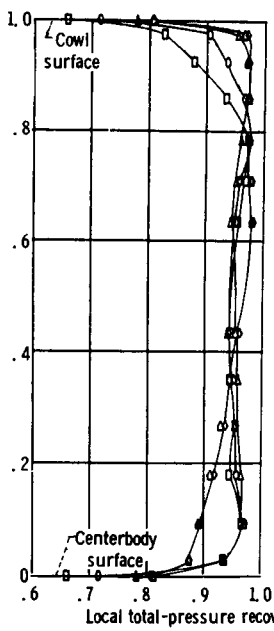
(a) Internal cowl surface pressure distributions.



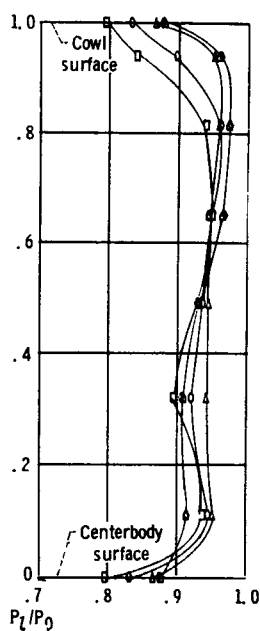
(b) Centerbody surface pressure distributions.



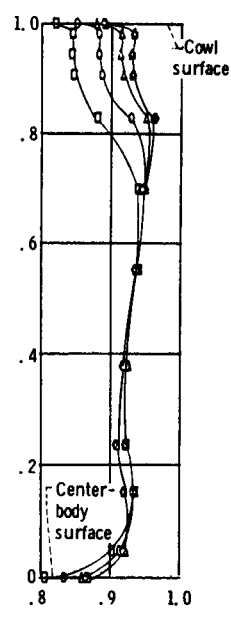
(c) Boundary-layer rake profiles.



(d) Throat-exit rake profiles.

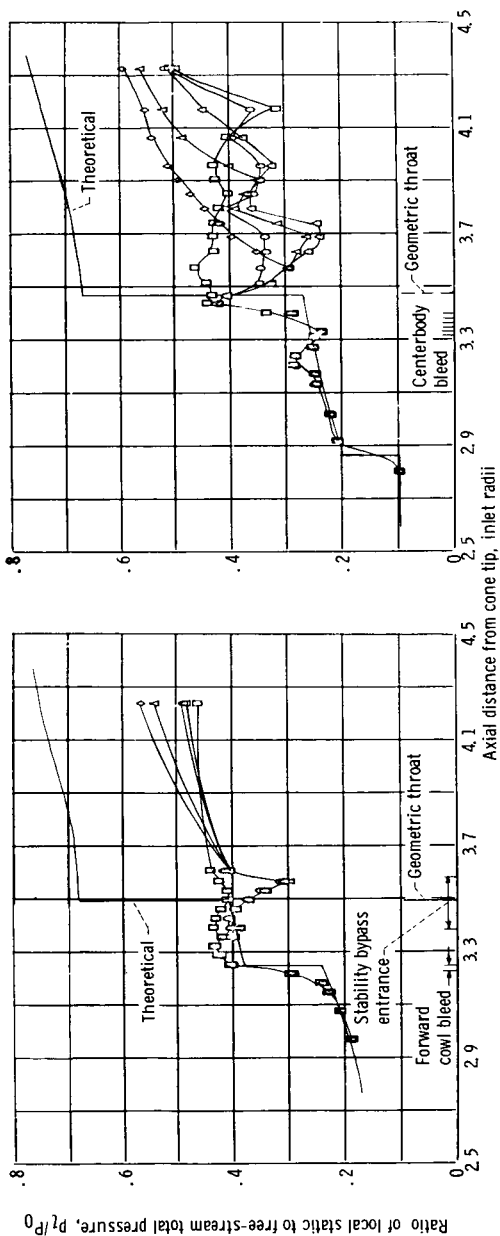


(e) Mid-diffuser rake profiles.



(f) Typical diffuser-exit rake profiles.

Figure 17. - Diffuser static- and total-pressure distributions for configuration NH-3 at minimum stable operation.

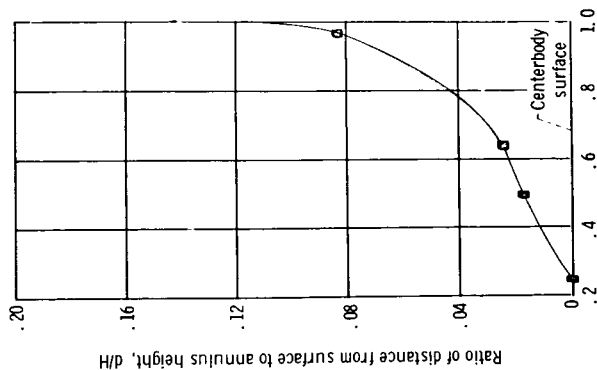


(a) Internal cowl surface pressure distributions.

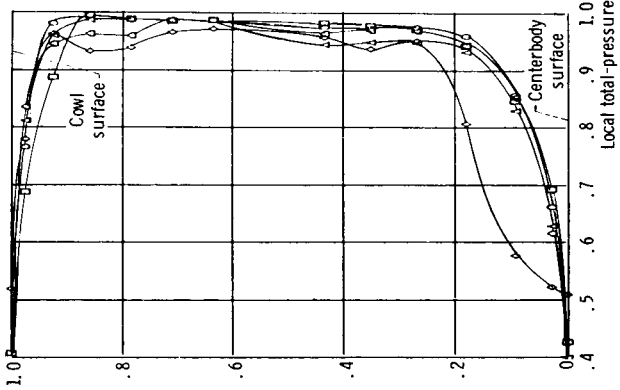
(b) Centerbody surface pressure distributions.

Mass-flow ratio, $m_5/m_0$	Total-pressure recovery, $P_5/P_0$	$P_{5b}/P_0$
0	0.941	0.853
0.2	0.923	0.850
0.4	0.891	0.844
0.6	0.871	0.841
0.8	0.860	0.806
1.0	0.806	0.143

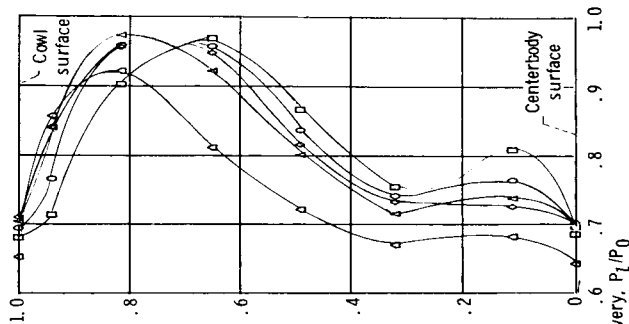
Symbols at 0 and 1.0 d/H indicate static pressures



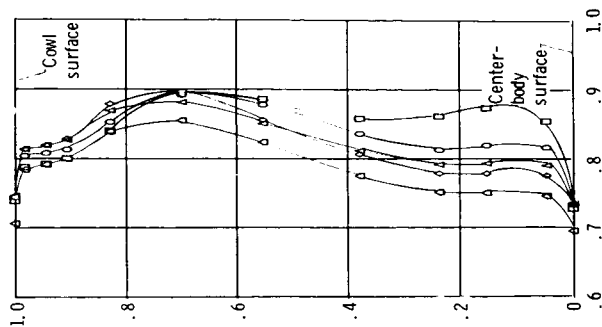
(c) Boundary-layer rake profiles.



(d) Throat-exit rake profiles.



(e) Mid-diffuser rake profiles.



(f) Typical diffuser-exit rake profiles.

Figure 18. - Diffuser static- and total-pressure distributions for configuration NH-3 at supercritical operation.



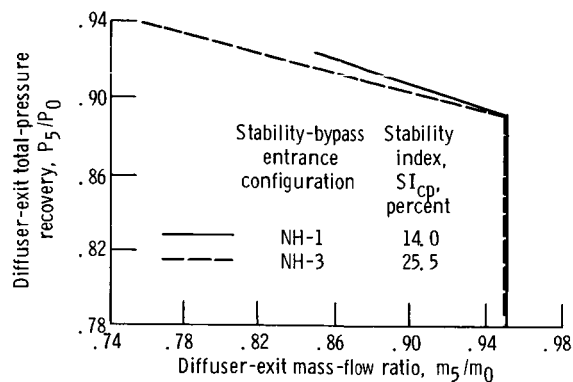
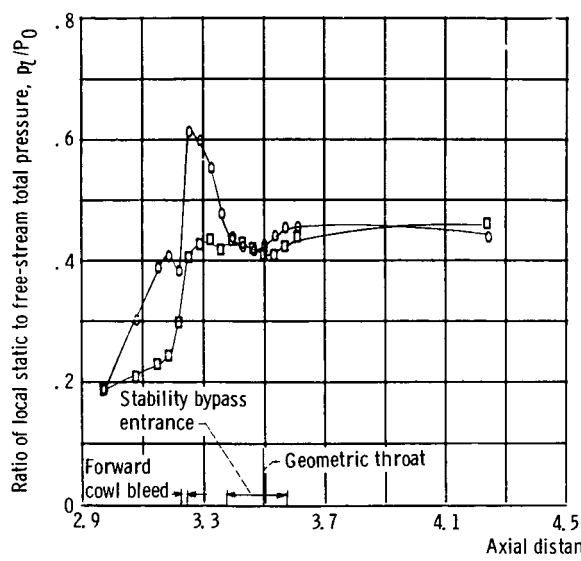
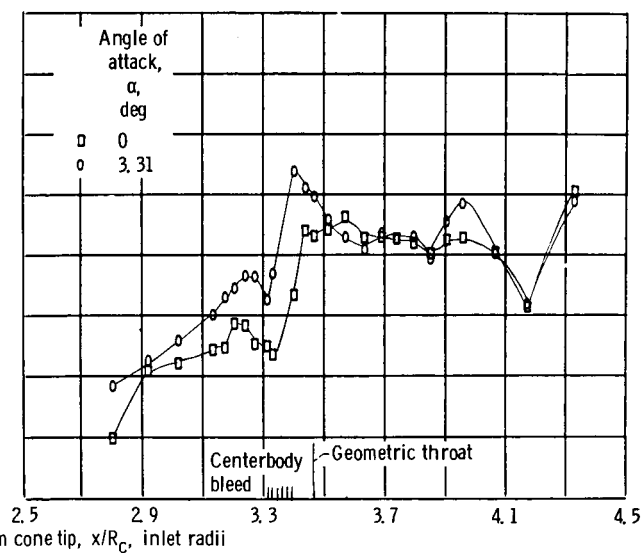


Figure 19. - Comparison of inlet performance based on constant stability-bypass recovery to unstart limit from initial inlet conditions of 89 percent total-pressure recovery and total forward cowl bleed and stability-bypass mass-flow ratio of 0.02. Free-stream Mach number, 2.50; angle of attack,  $0^\circ$ ; overboard-bypass mass-flow ratio, 0.01.



(a) Internal cowl surface pressure distributions.



(b) Centerbody surface pressure distributions.

Figure 20. - Static-pressure distributions at  $0^\circ$  angle of attack and maximum angle of attack prior to unstart. Configuration NH-3.